DOI: 10.1002/adma.XXXX
Article type: Review

Functional Single-Walled Carbon Nanotubes and Nano-Engineered Networks for Organic and Perovskite Solar Cell Applications

David R. Barbero and Samuel D. Stranks*

David R. Barbero
Nano-Engineered Materials and Organic Electronics Laboratory, Umeå Universitet, Umeå 90187, Sweden
* Email: david.barbero@umu.se

Samuel D. Stranks
Research Laboratory of Electronics, Massachusetts Institute of Technology, Cambridge, MA, 02139, USA
Cavendish Laboratory, JJ Thomson Avenue, Cambridge CB3 0HE, United Kingdom

Keywords: carbon nanotubes network, nano-engineering, charge transport, organic electronic devices, nanoimprinting, nano-structures, polymer wrapping, perovskite solar cells

---

Authors' Biographies

David R. Barbero performed his PhD at the Cavendish Laboratory, University of Cambridge, where he was a Marie-Curie Fellow and a European Cambridge Trust Scholar. He was awarded the Abdus Salam runner-up prize in 2009 from the Cavendish Laboratory for his PhD work. Shortly afterwards, in 2010, he became Assistant Professor in Physics at Umeå University, Umeå, Sweden and head of the Nano-Engineered Materials and Organic Electronics Laboratory. His interests are in the physics of confined and nanoscale systems, nanofabrication methods, nanocomposites made of polymers and nanocarbon materials, as well as their application to photovoltaics and other optoelectronic devices.

David R. Barbero

Samuel D. Stranks is a Marie Curie Fellow based jointly at the Massachusetts Institute of Technology and the University of Cambridge. He completed his PhD in 2012 as a Rhodes Scholar at Oxford University, working on carbon nanotube/polymer blends with Robin Nicholas. He then worked as a post-doctoral researcher in Henry Snaith's group at Oxford University where he was also a Junior Research Fellow at Worcester College. His research generally focuses on the optical and electronic properties of emerging photovoltaic and optoelectronic systems, particularly metal halide perovskites and carbon nanotubes.

Abstract

Carbon nanotubes have a variety of remarkable electronic and mechanical properties that in principle lend them to promising optoelectronic applications. However, the field has been plagued by heterogeneity in the distributions of synthesized tubes and uncontrolled bundling, both of which have prevented nanotubes from reaching their full potential. In this progress report, we present a variety of recently-demonstrated solution processing avenues that could combat these challenges through manipulation

Samuel D. Stranks

of nanoscale structures. We show recent advances in polymer-wrapping of single-walled carbon nanotubes (SWNTs) and how the resulting nanostructures can selectively disperse tubes while also exploiting the favorable properties of the polymer such as light harvesting ability. We also discuss new methods to controllably form nano-engineered SWNT networks with controlled nanotube placement. These nano-engineered networks decrease bundling, lower the percolation threshold and enable a strong enhancement in charge conductivity compared to random networks, making them potentially attractive for optoelectronic applications. Finally, we review SWNT applications to date in organic and perovskite photovoltaics, and we provide insights as to how the aforementioned recent advancements could lead to improved device performance.

1 Introduction

Since the early 1990s, the production and the characterization of carbon nanotubes' properties and their potential applications have increased dramatically. Carbon nanotubes are among the stiffest, toughest, strongest and most resilient materials known to man. Investigation of their mechanical properties by transmission electron microscopy (TEM) and by atomic force microscopy (AFM) have revealed that individual carbon

nanotubes have a Young's modulus in the TPa range, and a bending strength over 14 GPa. [1–4] For this reason, they have been widely investigated in composites to reinforce a polymer matrix to make it stiffer and more resistant to deformation. [5, 6] Moreover, the exceptional electrical properties and high charge carrier mobility of carbon nanotubes (CNTs) lends them to application in a range of devices including high-performance transistors, supercapacitors, electrically conductive adhesives, piezoresistive polymer composites and flexible optoelectronic devices. [7–12]

Single-walled carbon nanotubes (SWNTs), which are made of a monoatomically thin sheet of graphene rolled-up in a quasi 1 dimensional cylinder, are particularly attractive due to their large aspect ratios and remarkable electronic and transport properties. SWNTs, whose diameters range from less than a nanometer to several nanometers, were first reported independently in 1993 by Iijima and by Bethune. [13, 14] The way the graphene layer is rolled-up determines the nanotube chirality and diameter, which in turn dictates the electronic character of the SWNT as either metallic or semiconducting. [15] **Figure 1** shows a graphene sheet which, when rolled up along one of the chiral vectors, forms a specific type of SWNT (zig-zag, armchair, chiral) denoted by their chiral indices (n, m), with each having unique electronic properties. Experiments on individual metallic tubes and small bundles of SWNTs have demonstrated very high conductance and ballistic charge transport. [16–18] These results indicate that metallic SWNTs can therefore conduct electricity as well as the best metals, even at room temperature. Moreover, due to a typically low defect density compared to metals, charges in metallic tubes exhibit much longer mean free paths on the order of microns. [19, 20]

The semiconducting behavior of SWNTs was first reported in 1998 [21] where a nanotube was deposited between source (S) and drain (D) contacts, and the gate voltage V_g was varied between negative and positive values. Measurement of the conductance between S and D revealed that charges were transported through the nanotube only

at negative gate biases, essentially behaving as a p-type metal-oxide-semiconductor field effect transistor (MOSFET). They have since been intensely investigated for their semiconducting properties which have promised highly performant electronic devices, such as hybrid SWNT photonic crystals, broadband photodetectors, all-carbon photovoltaic solar cells, and photothermal nanotube/polymer composites for biomedical applications. [22–32] Moreover, their high surface area to mass ratio (1600 m^2/g) makes them sensitive to adsorbed species and attractive for gas sensor applications. [33, 34]

In this Progress Report, we discuss functional SWNTs, especially nanotubes wrapped with a semiconducting polymer, and the integration of SWNTs into thin-film devices. We will moreover focus on the formation and properties of novel types of nanotube networks: nanoscale nano-engineered SWNT networks. This new concept has shown tremendous potential for producing high-performance optoelectronic devices which effectively exploit the intrinsic nanotube properties and use reduced amounts of nanotubes compared to random networks. We finally review and comment applications of functional SWNTs and nano-engineered networks in the emerging fields of nanocarbon and perovskite photovoltaics.

2 Tailored electronic properties by sorting, doping and wrapping of SWNTs

2.1 Methods for sorting and dispersing individual tubes

The synthesis of SWNTs generally produces insoluble bundles consisting of a mixture of different chiralities of both semiconducting and metallic nanotubes. Moreover, control of the tube diameter is important for electronic applications because the band gap and carrier mean free path of the nanotubes vary with the diameter. [36] For optoelectronic applications, the tubes need to have controlled electronic properties in order to produce devices with reproducible characteristics. The ensemble of different

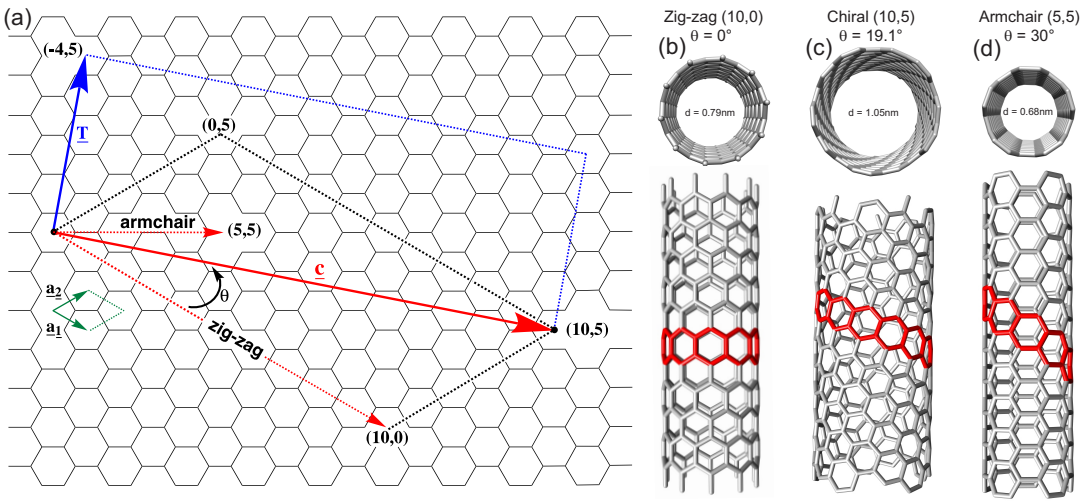

Figure 1: Representation of chiral vectors leading to various types of SWNTs. (a) The chiral vector $c = 10a_1 + 5a_2$ (red arrow), defined by the two basis vectors a_1 and a_2, joins two points on a graphene sheet, and forms the circumference of a (10,5) nanotube. The chiral angle θ, and the chiral vectors which specify zig-zag (10,0) and armchair (5,5) nanotubes are shown (red dotted arrows).(b,c,d) Examples of zig–zag, chiral and armchair SWNTs, with their angle θ and diameter, d. From [35]

tubes makes characterization and repeatable device preparation difficult. Furthermore, metallic nanotubes can be detrimental to optoelectronic device performance because their lack of bandgap can lead to quenching of excitons and charges in devices, for example. [37] For these reasons, post-synthesis sorting methods such as gel chromatography [38] or density-gradient ultracentrifugation (DGU) [39] have been developed to sort and select a specific type of nanotube with similar characteristics and properties. In DGU individual nanotubes are sorted from subtle differences in their densities when dispersed by a range of surfactants, and this method has been successfully used to separate tubes by diameter, length or electronic type (see **Figure 2**). [39] However, these methods are typically complex or require specialized equipment.

The scalable synthesis of single chirality nanotubes still remains an elusive goal, though recent reports towards this end are encouraging. Liu et al. demonstrated a strategy using an initial chirality-sorting step to obtain tubes to serve as starting templates for an ensuing chirality-controlled nanotube cloning process. [40] Yang et

al. showed that SWNTs of a single (12,6) chirality could be directly produced with an abundance of 92% using tungsten-based bimetallic alloy nanocrystal catalysts. [41] Sanchez-Valencia demonstrated controlled growth of defect-free single chirality (6,6) nanotubes seeded on a platinum surface and subsequently elongated to a few hundred nanometers. [42]

Nanotube solubility in solvents is generally very low with many of the tubes existing in bundles. [43] The highest nanotube solubility (cyclohexylpyrrolidone, CHP) is 3.5mg/mL, though even in such a good solvent small bundles still remain [44]. In order to increase nanotube solubility and reduce bundle formation, both covalent and non-covalent functionalization methods have been used. In the covalent method, the surface of the nanotube is chemically modified, typically by either oxidation or chemical reaction in acidic solutions, to covalently attach functional groups. [45–47] While this approach leads to stable chemical modification of the tube, and produces dispersions which are stable in time, it also usually introduces structural defects and deteriorates the physical properties of the tubes (e.g. tube shortening, modification of its intrinsic electrical and/or spectroscopic properties). [48, 49] For this reason, non-covalent functionalization, through the use of π molecular (e.g. polymers) or hydrophobic (e.g. surfactant) interactions, is generally preferred in order to retain the nanotube's intrinsic properties and prevent structural damage. A breakthrough came in 2002 when O'Connell *et al.* were able to use ultrasonication to break up nanotube bundles and disperse the individual tubes through micelle formation with an aqueous surfactant [50]. The micelles prevent the nanotubes from rebundling and ultracentrifugation allows removal of the higher density micelles containing bundles from the lower density micelles containing individual tubes. Thus, by eliminating the rapid energy transfer within bundles from semiconducting to metallic nanotubes on which excitons recombine non-radiatively [51], photoluminescence (PL) from individual nanotubes was observed for the first time. This breakthrough also opened up the use of photoluminescence exci-

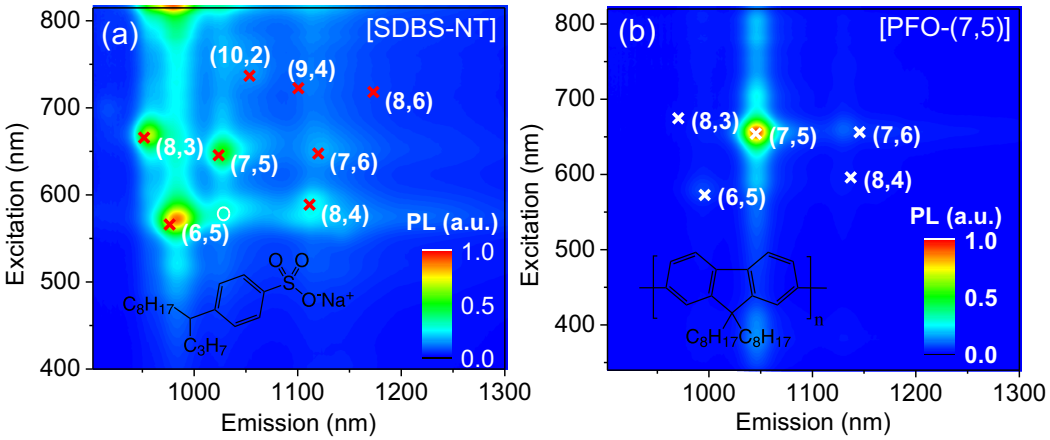

Figure 2: Photoluminescence excitation (PLE) maps of different nanotube distributions. PLE map of the (a) nanotube distribution dispersed with the surfactant Sodium Dodecyl Benzene Sulfonate in D_2O and (b) [PFO-NT] nanohybrids in *o*-xylene. The SWNT species (red crosses) are assigned using the Weisman and Bachilo empirical model [52], and those in (b) are globally red-shifted by 25 meV to approximately account for the effect of a changed environment on the transition energies [53]. A tube-tube energy transfer process is highlighted with a white circle.

tation (PLE) spectroscopy as a powerful tool to characterize nanotube distributions. Here, the sample is excited with visible light corresponding to the second lowest exciton transition (E_{22}) in semiconducting tubes, and the emission in the near-infrared from the lowest exciton transitions (E_{11}) is detected. The sets of transitions (E_{11},E_{22}) provide a unique fingerprint of each (n, m) semiconducting nanotube in a distribution, as shown in a PLE map in Figure 2(a).

O'Connell *et al.* first demonstrated that conjugated polymers can also bind to nanotubes via strong π-π interactions and efficiently disperse tubes. [54] The non-covalent nature of the polymer binding means that the intrinsic properties of the tubes can be preserved while utilizing the favorable properties of the polymer. The solution processing steps for state-of-the-art polymer wrapping and purification are summarized in Figure 3(a). The polymer and nanotubes are mixed in an organic solvent and briefly treated in an ultrasonic disintegrator to break up bundles and allow the polymer chains to interact with the tube surfaces. This is followed by ultracentrifugation to induce

precipitation of any unbundled tubes, while the polymer-wrapped tubes (nanohybrids) remain dispersed in the supernatant, which is retained. [55, 56] In order to remove the excess polymer and purify the nanohybrids, aggregation of the nanohybrid species is induced by addition of an orthogonal solvent such as toluene. [57] The aggregated nanohybrids are recovered as a residue by ultracentrifugation, while the unbound polymer remains in the discarded supernatant solution. The purification can be repeated several times by redispersing the residue in the orthogonal solvent and re-centrifuging. The final purified residue can be dispersed in any desired solvent to any concentration.

There is a wide range of polymer families available to wrap the tubes. [60] These polymers can be chosen either for their favorable optical, electrical and mechanical properties or for the strong binding selectivity they have for certain tubes in the distribution. [59] Nish *et al.* showed that polyfluorene polymers preferentially bind to certain semiconducting nanotube species [55], such as (7,5) tubes (Figure 2(b)). This allows exclusion of other species such as metallic nanotubes using simple solution processing techniques. We recently exploited this selectivity to selectively wrap semiconducting tubes with desired polymers, as described in Section 2.3 below (Figure 3(b)). [58, 59] Toshimitsu and Nakashima also reported the separation of metallic and semiconducting SWNTs using metal-coordination polymers (CP-M) with M= Co, Ni, Cu or Zn. [61] We summarize the chirality selectivity of selected polymers in Table 1.

2.2 Semiconducting properties and doping of SWNTs

Both p-type and n-type behavior has been observed in semiconducting SWNTs, which largely depend on the alignment of the Fermi level with respect to the frontier orbital energies of the nanotube. Doping by injecting the appropriate charge carriers into either the valence or conduction bands of the nanotube can be achieved by different strategies, e.g. by tuning the work function of the electrodes contacting the nanotubes,

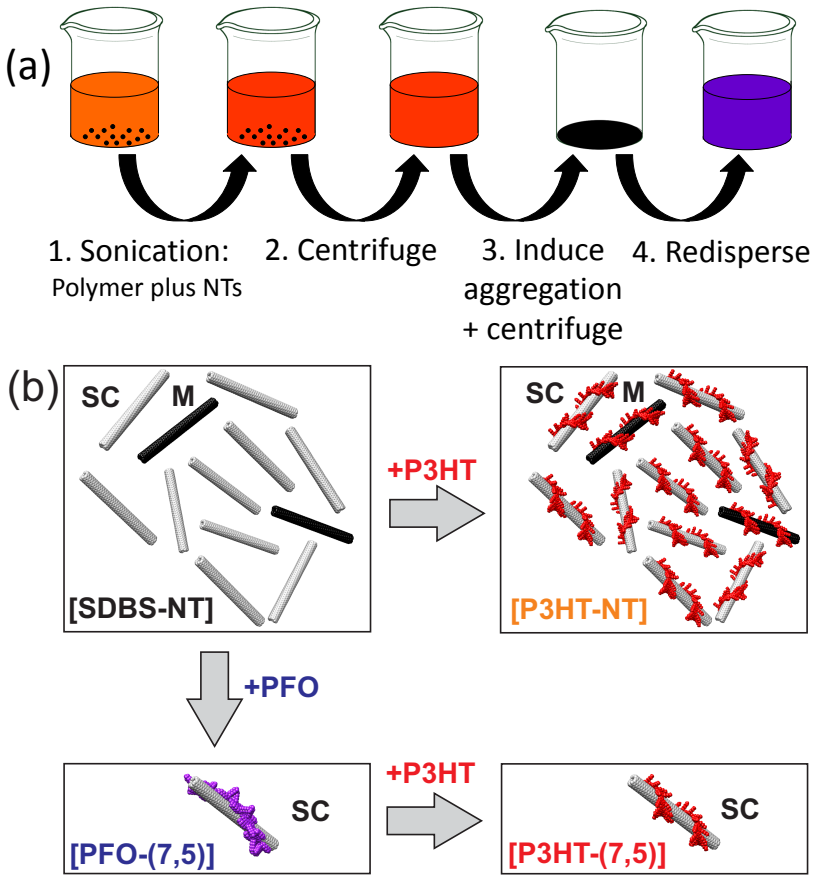

Figure 3: (a) Solution-processing steps to synthesise and purify polymer-wrapped carbon nanotube dispersions. (b) Scheme to illustrate different polymer exchange sample preparation routes [58,59]. The starting material, containing both metallic (M) and semiconducting (SC) tubes, can be dispersed in SDBS to give [SDBS-NT] nanohybrids. The tubes can also be directly dispersed with P3HT, termed [P3HT-NT], retaining all of the original species. Alternatively, the (7,5) SC tubes can be selectively wrapped by dispersion in PFO, [PFO-(7,5)]. The PFO can then be displaced by P3HT, giving [P3HT-(7,5)] nanohybrids.

or by adsorption of chemical dopants as discussed below. Optoelectronic and electronic devices based on carbon nanotubes often require doping which can tune the majority charge carrier type (n- or p- type) and the Fermi energy level. [62,63] Doping of SWNTs has been used to produce chemical sensors, and to shift the voltage at which a carbon nanotube transistor turns ON and OFF. [64, 65] Exposure to oxygen has been shown to p-dope SWNTs, while heating and exposure to UV radiation lowers the level of p-doping. [66] N-doping has been achieved by non-covalent functionalization with electron donating species such as alkali metals and organic materials such as polymers, and applied to the formation of n-type transistors and p-n junctions. [16, 62, 64, 67] Both small molecules and large macromolecules, e.g. gas molecules, organic and metallic molecules, polymers, can be used to efficiently transfer charges to nanotubes. Metallic dopants have been used to transfer charges to carbon nanotubes and graphene, due to the difference in workfunction between the graphene sheet and the metal. Moreover, the self-assembly of both small and large organic molecules, through π-π interactions with the surface of the nanotube, has recently emerged as a powerful way to transfer charges from an electron-donating species to an electron-accepting material (**Figure 4**). This type of functionalization relies on the physisorption of molecules onto the surface of either nanotubes or graphene sheets, and it has enabled both p-type [68–70] and n-type doping [68, 70–73].

2.3 Functionalization of SWNTs by polymer wrapping

Wrapping of macromolecules around carbon nanotubes (either MWNTs or SWNTs) in order to promote photoexcited charge or exciton transfer between the two materials have been demonstrated with poly(phenylacetylene)s (PPAs), an electron-donating pi-extended tetrathiafulvalene (exTTF), and many other semiconducting polymers including polyfluorene (PFO), poly-3-hexylthiophene (P3HT) and poly(9,9'-dioctylfluorene-*co*-benzothiadiazole) (F8BT). [74–76] The primary factors determining photoexcited

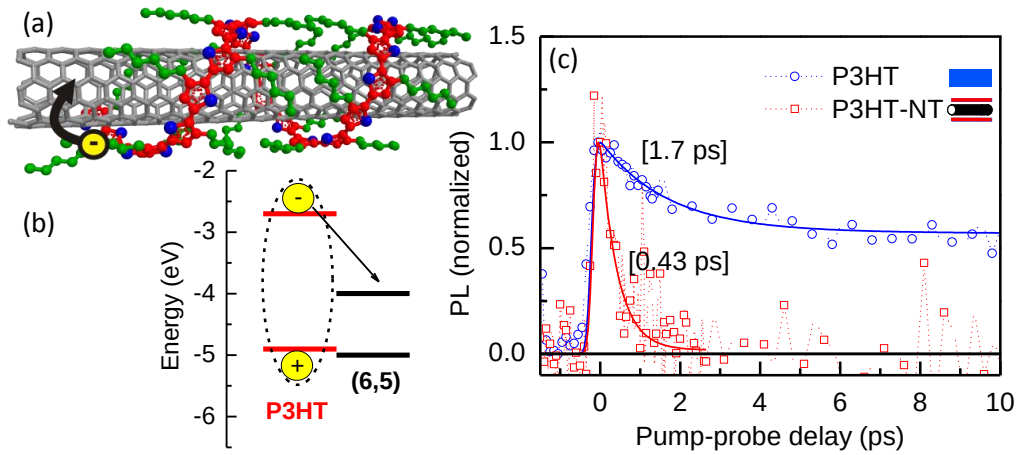

Figure 4: (a) Schematic diagram of a (6,5) SWNT coated with a monolayer of sheath P3HT, with electron transfer from P3HT to the SWNT. Sulfur atoms are colored blue, the carbon backbone is red and the side-chains are green. (b) The type-II heterojunction between P3HT and a (6,5) nanotube and charge transfer, which competes with energy transfer. Energy levels were taken from Ref. [53]. (c) Normalized time-resolved photoluminescence measurements for the [P3HT-NT] and P3HT samples following 400-nm sample excitation. Appropriate fits give fast time constants of 0.43 and 1.7 ps for [P3HT-NT] and P3HT samples, respectively, including a slow component for the P3HT sample only.

electron, hole or exciton transfer are the relative energies of the frontier orbitals (valence and conduction bands) of both the wrapping polymer and the semiconducting SWNT. Selective charge transfer is desired over exciton (energy) transfer at the interface to ensure effective charge separation of electrons and holes to opposite electrodes in a photovoltaic (PV) device, thus generating a photovoltage and photocurrent.

When a monolayer of most light absorbing molecules are physisorbed onto a SWNT, a type-I interface forms which facilitates energy transfer from molecule to SWNT. However, a type-II staggered interface can form between some molecules such as P3HT polymers and small-diameter semiconducting SWNTs, which makes charge transfer from molecule to SWNT favorable (Figure 4b). [53] We have shown that in this situation, photo-generated excitons dissociate at the interface and electrons transfer from P3HT to the nanotube on an ultrafast time scale ($\sim$ 430 fs) [77] (Figure 4c). In the presence of an excess P3HT network, charge separation at room temperature is long-lived and comparable to that in a conventional P3HT-fullerene blend. [77] Others have re-

Type of tubes (Manufacturing process)	wrapping polymer (non-covalent)	selectivity (majority chirality)	references
SWNT (CoMoCAT)	PFO	S; (7,5)	[55, 58]
SWNT (CoMoCAT)	P3HT	none	[57, 77]
SWNT (CoMoCAT)	F8BT	weak	[58, 78]
SWNT (HiPCO)	PFO	S; (8,6)	[55]
SWNT (HiPCO)	P3DDT	S; several	[79]
SWNT (HiPCO)	CP-M	S; several	[61]
SWNT (HiPCO)	P1	weak	[80]
SWNT (HiPCO)	MEHPPV	weak	[78]
SWNT (HIPCO)	ex-TTF	weak	[75]

Table 1: Summary of non-covalent methods to functionalize carbon nanotubes. Selectivity to a specific type of tube is indicated by M (metallic) or S (semiconducting). Acronyms: PFO (polyfluorene); P3HT (poly-3-hexylthiophene); F8BT (poly(9,9-dioctylfluorene-co-benzothiadiazole)); P3DDT (poly(3-dodecylthiophene)); MEHPPV (poly[2-methoxy-5-(2-ethylhexyloxy)-1,4-phenylenevinylene]); ex-TTF (pi-extended tetrathiafulvalene); CP-M (metal coordination polymer); P1 (poly[(9,9-dihexyl-2,7-fluorene)-1,4-(1,2,3-triazole)).

ported similar charge transfer effects between P3HT and nanotubes. [81–83] and similar time scales of charge transfer have also been reported for quantum dot (CdS)-SWNT nanocomposites, with measurable photocurrent generated from the junction. [84] We have also shown that an additional polymer can be introduced to form coaxial SWNT-dual polymer nanostructures, thus enabling further control of the electronic properties by molecular engineering of the structures to give specific attributes, such as prolonging stabilized charge separation or charge confinement. [59, 85] Recently, conjugated polymers made of alternating 9,9-dialkyl fluorene and 1,2,3-triazole units, demonstrated good selectivity to SWNTs by wrapping preferentially to specific chiralities, e.g. (8,6) tubes. [80] These discoveries open up the possibility to use polymer-functionalized SWNTs as efficient absorbers and charge transfer hybrid materials for application in,

among others, photovoltaics. This will be discussed in more detail in Section 4.

The semiconducting polymer PFO and similar polymers that are able to impart tube selectivity (see Section 2.1) typically have large bandgaps and low mobilities and therefore the additional function these polymers themselves add to optoelectronic applications is limited, for example as solar light harvesters. On the other hand, most polymers (with very few exceptions [79]) that have higher mobilities and lower bandgaps, for example suitable for solar light harvesting, such as P3HT wrap all tubes indiscriminately. For nanotube–polymer blends to find ultimate optoelectronic application, the polymer with desired mechanical and electrical properties must coat only a single chirality of semiconducting nanotube. Towards this goal, we recently developed a 'polymer exchange' method in which we first utilize the PFO-dispersing process to select predominantly (7,5) semiconducting SWNTs from a distribution. [58, 59] The wrapping PFO polymer is then entirely substituted by a preferable polymer in solution (Figure 3(b)). As first examples, this was demonstrated for P3HT and F8BT polymers, which have been widely used for photovoltaic and light-emitting applications, but the method could equally be applied using other desirable polymers.

3 Formation of electrically conductive SWNT networks and thin films

3.1 Electrical percolation of nanotubes

Due to their exceptional ability to transport charges, nanotubes can act as highly efficient charge transport pathways inside an insulating or semiconducting matrix, such as a polymer. However, one important condition for efficient and optimal charge transport is the ability to form a continuous (percolated) network of interconnected tubes inside the polymer matrix. Here we focus on carbon nanotubes mixed in solution with a polymer, and deposited onto a substrate, as opposed to tubes grown directly onto a

substrate. This approach offers ease of processing in select solvents, fine tuning of the SWNT concentration, and the choice of either rigid or flexible, insulating or conducting, substrates. The mechanical, thermal and electrical properties of nanotube composites are drastically changed when the particles reach a minimum concentration inside a composite medium in the solid state, e.g. a polymer. This limit, called percolation threshold (ϕ_c), is the concentration at which the particles connect each other in such a way that they form a continuous path which conducts electrical charges through the composite. The shape (tube, sphere etc.), aspect ratio and interaction potential of the particles strongly influence the formation of the network and the percolation threshold in a given matrix. Weakly interacting nanotubes tend to form locally and globally isotropic random networks (**Figure 5** a), whereas more strongly interacting tubes are expected to produce locally anisotropic but globally isotropic networks (Figure 5 b). [86] A typical random network of SWNTs, formed by deposition from solution, is displayed in Figure 5 c. [87] As the aspect ratio (A_r) of the randomly oriented particles increases above 10, the minimum concentration to reach percolation rapidly decreases (Figure 5 d). This result can be explained by the excluded volume theory which predicts that the average number of connections per particles is proportional to the excluded volume V_{ex} (Eq. 1) [88–91], defined as the volume around the center of a particle which cannot be crossed by another particle in order to prevent interpenetration of the two particles. In the case of carbon nanotubes, which can be considered as long and flexible cylinders, only a small addition of nanotubes is typically necessary to reach percolation due to their large aspect ratio which can exceed 1000.

The excluded volume is defined as:

$$V_{ex} = 2d\,[\frac{2\pi}{3}d^2 + \pi dL + L^2 < sin\gamma >] \tag{1}$$

where d and L are the diameter and the length of the nanotube, and γ is the angle between two nanotubes. Moreover, the state of dispersion of the nanotubes (e.g. random

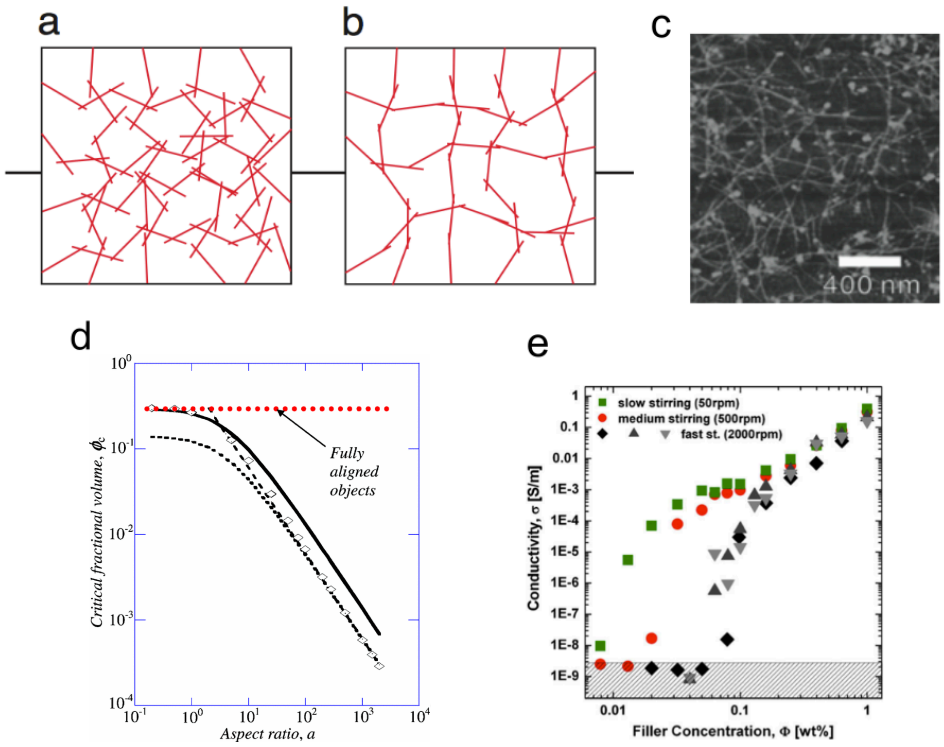

Figure 5: Percolation of nanotubes. Models of a) locally and globally isotropic percolation of tubes; and b) locally anisotropic but globally isotropic (from Bisri et al., [87]). c) SEM image of a random network of SWNTs spun from solution; scale bar is 400 nm. From Bisri et al., [87]. d) Critical fractional volume ϕ_c of randomly oriented soft-core sticks vs. aspect ratio for 3D systems. [92] e) Conductivity of a MWCNT/epoxy nanocomposite as a function of the nanotube filler concentration for three different sample preparation methods: slow (50rpm), medium (500rpm), and fast (2000rpm) stirring of the dispersion. [93]

vs. aligned) also has a strong influence on the percolation threshold. Typically, aligned objects will reach percolation at a higher fractional volume compared to randomly oriented objects due to the reduced number of connections in the direction perpendicular to their alignment. [92, 94, 95]

The problem of percolation is important for determining when a network of nanotubes, in a dispersion or in a thin-film composite, becomes electrically conductive. In the vicinity of the percolation threshold ϕ_c, the conductivity σ varies with the volume fraction of fillers ϕ as:

$$\sigma(\phi, A_r) = \sigma_0 \left[\phi - \phi_c(A_r)\right]^t \tag{2}$$

where σ_0 represents the intrinsic conductivity of individual nanotubes or clusters, and t is an exponent which depends on the aspect ratio A_r of the filler, and on the dimensionality of the conductive network. For 3D networks, the exponent t typically varies between 1.8 and 2.3 for low aspect ratio objects, averaging t=2.0 for a sphere, and dropping to t=1.2–1.3 for large aspect ratios A_r>500–1000 such as SWNTs. [92] σ_0 can be estimated by the following equation for a 3D system:

$$\sigma_0 = \left(R_0 \, L \, \phi_c^t\right)^{-1} \tag{3}$$

where, R_0 is the resistance of an individual nanotube, or of the contact between nanotubes if this value is greater. Typical values for individual SWNTs for L≈1000 nm were measured to be R_0≈10^4–10^5 Ω. [96] The resistance R_0 increases with the length of individual tubes, and also with the number of contacts formed with other tubes inside a network. Both SWNT resistance R_{SWNT} and contact resistance $R_{contact}$ were recently measured by conducting atomic force microscopy (c–AFM), and gave values of R_{SWNT}≈ 3–16 $.10^3$ Ω/μm, and $R_{contact}$≈ 29 $.10^3$ Ω for a junction formed by 10 nm bundles. [97] It should also be noted that in the case where nanotubes do not form a direct contact with each other, but instead are separated by a short distance (a

few nanometers), tunneling between nanotubes can occur. This will add a tunneling resistance to the network, and reduce the overall network conductivity compared to a network where tubes are in direct contact. [98, 99] Values of R_0 as high as 10^{13} Ω has been estimated in CNT composites where conductivity was controlled by tunneling. [92, 100]

The method used to form the nanotube network strongly influences its properties, including its percolation and its ability to transport charges. Percolation thresholds varying from 0.005 to 4–5 wt% have been reported for SWNTs mixed and dispersed by various methods (manual mixing, hot pressing, electrospinning, etc), and in different polymer matrices. [101–106]

Moreover, mechanical mixing can lead to a kinetic percolation, where CNTs are not necessarily randomly distributed inside the matrix. [93] The stirring speed of a carbon nanotube dispersion has been shown to strongly affect percolation, and slow stirring of a liquid multi-wall nanotube (MWNT)/epoxy solution resulted in a large decrease in ϕ_c compared to faster stirring, as illustrated in Figure 5 e. Fast stirring and high shear rates can indeed break the tube interconnections in the network and prevent charge transport at lower concentrations. When the concentration of filler reaches the value for the statistical percolation threshold, the effect of stirring however becomes negligible. [93]

3.2 Random network formation in thin films

Reducing the percolation threshold in functional materials, such as electrically conductive composites, is important for reducing costs of fabrication but also for ease of processing. In order to fabricate CNT-based electronic devices, the carbon nanotubes are typically deposited from solution on either a rigid or flexible substrate by spin-coating, drop-casting, or ink-jet printing. [10, 107–110] In the ink-jet and drop-casting methods, a drop of the dispersion of nanotubes in a solvent is allowed to evaporate

with or without heating. This results in a more or less uniform film of randomly oriented and randomly positioned nanotubes. In such random networks, the positioning and interconnection of the nanotubes with each other is usually not controlled. In the spin-coating method, the substrate is accelerated and spun at speeds of 500-10000 rpm right after deposition of a drop of CNTs mixed in a solvent. Fast acceleration evaporates the solvent, and forms a more uniform and thinner film than by drop-casting. However, because of the random nature of the nanotube network formed using these deposition methods, and the lack of controlled positioning of the nanotubes inside the film, these methods result in non-optimal charge transport properties and lower device performance than could be obtained by controlled network formation. [111] The randomness of the networks and non-ideal interconnection of tubes is illustrated in **Figure 6 a**, where it is evident that only a limited fraction of the nanotubes are interconnected and contribute to charge transport across the network. Moreover, random networks formed by drop-casting and spin-coating are mostly irreproducible, and they tend to produces bundles or agglomerates of nanotubes which increase junction resistance and further decrease the conductivity of the network. [103, 112–114] Using a floating catalyst synthesis and an aggregation chamber method, it was recently demonstrated that SWNT networks with smaller bundles formed better interconnected and more conductive networks. [115] The bundle size can be reduced by using appropriate surfactants in order to decrease the attractive force between tubes. A recent study showed the benefit of using specific surfactants with semiconducting SWNTs, which resulted in a finer network morphology and increased ON-OFF ratio and charge carrier mobility in thin film transistors. [116] Controlled dispersion of the nanotubes and formation of a continuous (percolated) network of interconnected tubes inside a polymer matrix is therefore important for better charge transport, for more reproducible electrical properties, and for improved device performance. Moreover, sub-optimal device performance and low carrier mobility has been attributed to the random nature of the nanotube

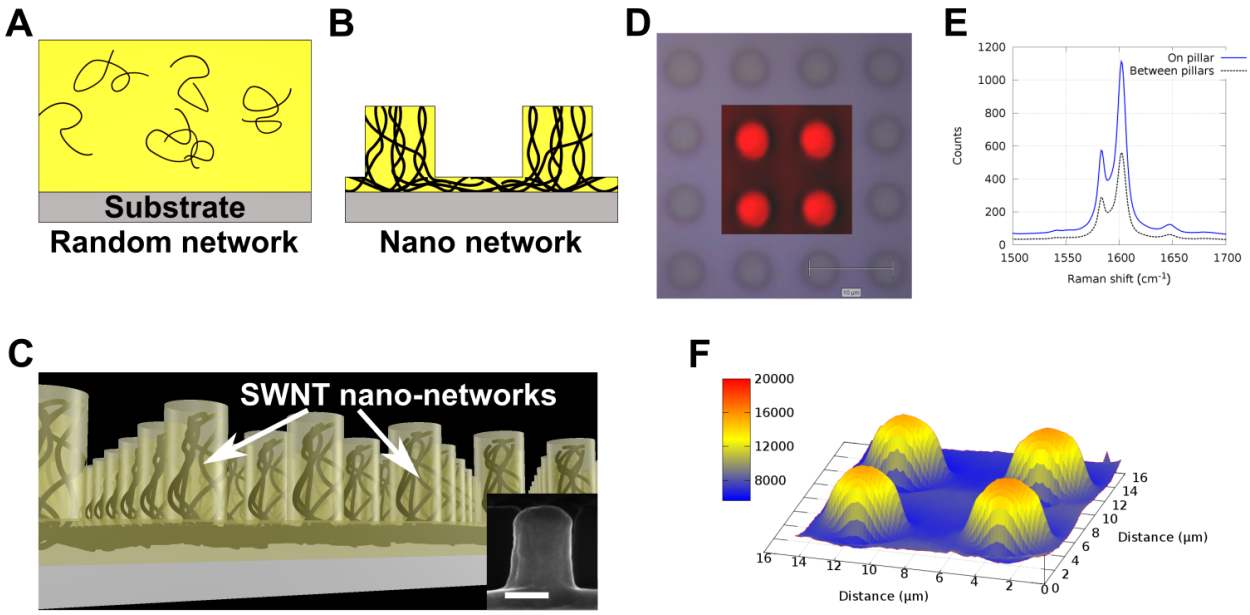

Figure 6: Nano-engineered SWNT networks in a thin polymer film. Difference in nanotube placement and network formation between random (a) and nano-network (b). (c) Schematics of the SWNT nano-network in a SWNT/polymer composite film, showing a regular array of nanosized composite patterns with SWNT networks of well defined dimensions (from N. Boulanger *et al. [117]) The insert in (c) is a SEM cross section of a nano-engineered SWNT/P3HT network, the scale bar is 200 nm. (d) 2D Raman mapping showing the periodical variation of the distribution of the nanotubes in the film with microsized networks, where brighter spots represent higher SWNT content. (e) a Raman spectrum showing the intensity of the SWNT G-band inside a pillar and in between pillars. (f) 3D representation of the Raman mapping, showing a higher SWNT content inside the microsized networks. Panels (d, e, f) from D. R. Barbero et al. [118]*

network. [111]

3.3 Controlled nanoscale network formation

In order to better control tube positioning and network formation, we have recently demonstrated a new method which enables the formation of percolated SWNT networks in well ordered nanoscale domains in a polymer thin film. [118] Figures 6 a,b schematically show the nanotube architecture in the different types of networks. In a random network produced by traditional methods (Figure 6 a), only a small proportion of the nanotubes contribute to the formation of a path between the top and the

bottom of the film. By contrast, in a nano-engineered network (Figure 6 b,c), a much larger proportion of tubes forms interconnected pathways. This results in controlled nanotube placement at the nanoscale, as shown by Raman spectroscopy of microstructured SWNT networks (Figure 6 d-f), and in a nano-sized network architecture with enhanced charge transport.

This novel type of network can be produced either from a solid composite layer by thermal treatment, or directly from solution at room temperature. In both cases, this results in ordered arrays of well controlled micro- or nano-scale SWNT networks as characterized by both scanning electron microscopy (SEM) and atomic force microscopy (AFM) (**Figure 7** a,b). These nano-engineered networks were shown to have exceptional ability to transport charges compared to random networks, due to the high level of interconnection between nanotubes inside the network. An increase in conductivity of the nano-engineered network by 2 orders of magnitude was measured in a P3HT/SWNT thin film with semiconducting nanotubes, and formed thermally. [117]. A further increase in network conductivity by 5 fold was recently obtained by using a novel solvent method to form the nano-engineered networks from solution at room temperature(Figure 7 c,d). [119] Moreover, the charge transport mechanism in the nano-engineered networks was found to be quasi-ohmic, due to the formation of well percolated pathways, whereas random networks displayed a conducting behavior far from ohmic (Figure 7 c). The increase in conductivity was attributed to a better tube dispersion inside the nano-network, and to a reduction in tube bundling and bundle size. [119]

Nano-engineering of SWNT networks has also been shown to strongly reduce the amount of nanotubes necessary to reach percolation, and form a conductive path inside the composite film. Percolation thresholds as low as $\approx 10^{-5}$ wt% have been demonstrated by forming nanostructured networks of SWNTs, which holds great promise for reducing the cost of electronic devices which use highly purified semiconducting nan-

otubes. [120] Moreover, the controlled placement of nanotubes with nanoscale accuracy could be advantageous to produce more efficient devices. This new type of network has the additional advantages of being formed in a controlled way, with well-defined dimensions and patterns which can be changed at will, and it yields reproducible electrical properties which are not readily achievable with random networks.

The nanoscale architecture of the SWNT network clearly plays a critical role in device performance. The ability to controllably produce well defined nanoscale networks of SWNTs with low loading while retaining high interconnectivity of nanotubes, instead of random tube distributions, is therefore highly important for better understanding percolation and network formation, and for developing more efficient and lower-cost electronic devices.

4 SWNT-based Optoelectronic Devices

4.1 Transparent, and flexible electrodes using carbon nanotubes

Optoelectronic devices require that one of the electrodes be transparent in order for light to either enter (e.g. PV solar cell) or escape (e.g. light-emitting diode, LED) the active layer of the device with little or no energy loss. Traditionally, a glass substrate onto which a thin layer of either indium tin oxide (ITO) or fluorine doped tin oxide (FTO) is used as the transparent electrode. Owing to their good chemical stability, very good electrical conductivity (1-10 Ω / $\square$), and their optical transparency in the visible spectrum, both ITO and FTO electrodes have been widely used for a large number of applications including LEDs, touch screens, flat panel displays, and PV devices. [121] However, the scarcity of some raw materials such as indium has driven the cost of ITO electrodes up, and pushed the search for alternative materials and cheaper ways to produce transparent electrodes. Graphene and carbon nanotubes have been among

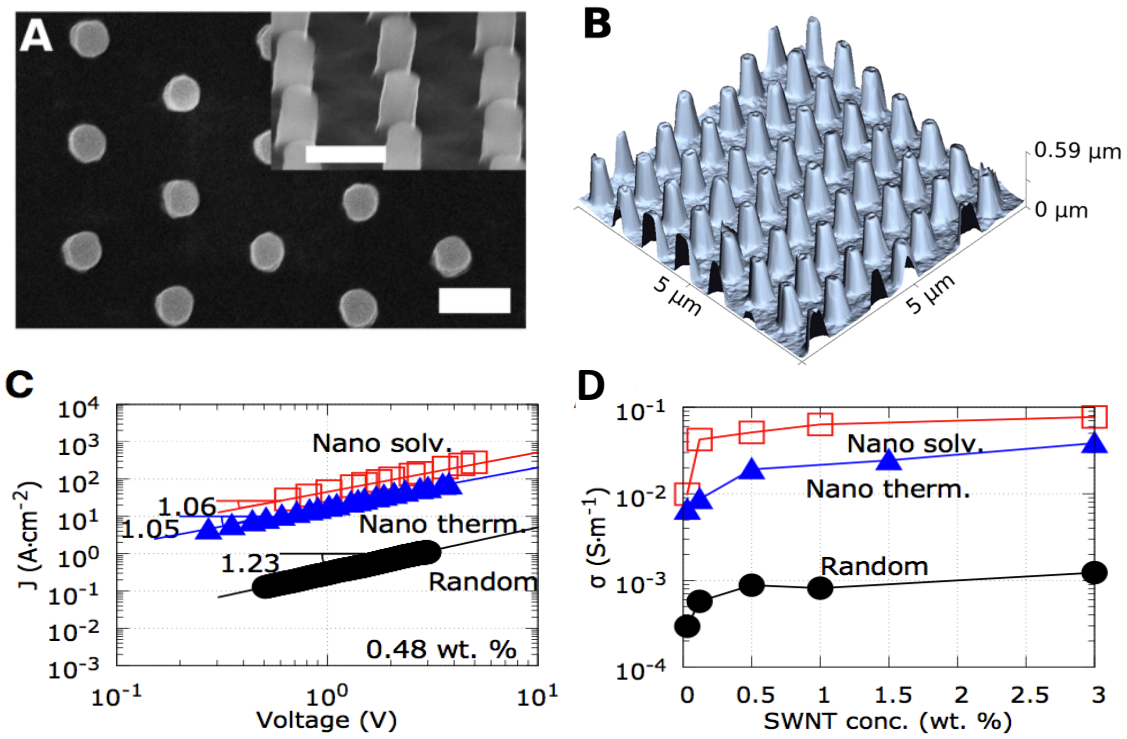

Figure 7: Structural and electrical properties of nano-engineered SWNT networks in a thin P3HT film. (a) Scanning electron microscopy (SEM) picture of the nano pillars from the top and from the side (tilted view). (b) 3D atomic force microscopy (AFM) imaging of the networks, and (c) J-V characteristics of different types of networks: random, thermally nano-engineered (nano therm.), nano-engineered from solution (nano solv.) at 0.48 wt.% of SWNTs. (d) Electrical conductivity as a function of the SWNT loading in the different types of networks. Scale bar in (a) is 500 nm. From N. Boulanger & D. R. Barbero [119].

the top contenders thanks to their exceptional charge transport, versatile processing methods and substrates, and good transparency when used in thin layers. [122, 123] Moreover, ITO and FTO electrodes are rigid and brittle, whereas nanocarbon materials (e.g. graphene and SWNTs) are flexible and they can be deposited on any surface, including flexible substrates. [124–129].

Transparent electrodes using conductive SWNT films have been demonstrated in a large number of studies, using either a rigid or flexible substrate, with typical values of the sheet resistance ≈60–200 Ω/□ for 80-90% transmittance at 550 nm. [10, 130, 132] Transmittance above 80% (in the visible region) for films deposited on a flexible polyethylene-teraphtalate (PET) plastic substrate had a sheet resistance of 150 Ω / □ (**Figure 8** a,b). [130] The nanotube film can be directly formed onto the substrate by different methods such as vacuum filtration or spin-coating from a solution in order to replace ITO or FTO. SWNT films made predominantly of sorted metallic (m) tubes are preferred in order to reduce the sheet resistance (R_{sh}). It was recently demonstrated that R_{sh} can be reduced 10 times in films made of m-SWNTs compared to films produced with a mixture of m- and s-SWNTs. [133] In the case of mixed nanotubes, long tubes with large diameters are usually preferable to reduce the band gap of s-SWNTs and increase the conductivity of the film. [134] It was also shown that films made of a large majority of s-SWNTs (>90%) can also be highly conductive due to the lowered junction resistance between s-SWNTs compared to that of m- and s-SWNTs in contact with each other. [135] A recent study moreover indicates that the electronic type of the nanotubes does not play as important a role as previously believed for making conducting electrodes. [136] Instead, the morphology of the SWNT film seems to play a critical role. In this work, the authors also demonstrated that the power conversion efficiency of an organic bulk heterojunction solar cell made with hole doped SWNT transparent electrodes was nearly as high as that made with ITO electrodes. In another study, graphene and SWNTs were combined into a single hybrid film, yielding a sheet resis-

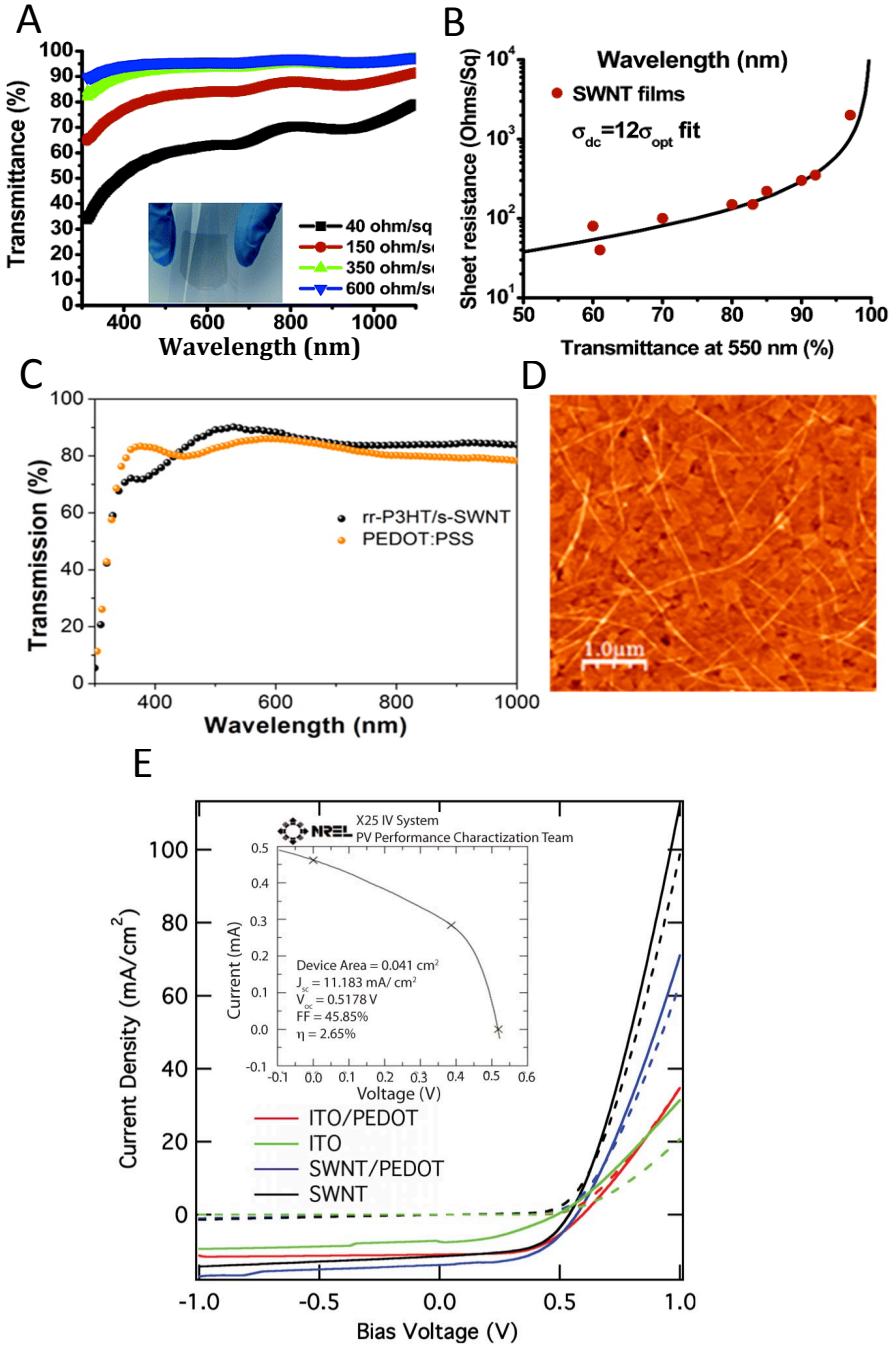

Figure 8: SWNT transparent electrodes. a) UV-vis-NIR transmittance of SWNT films of different thickness spun on a flexible PET substrate (inset), and corresponding sheet resistance (from Li et al., [130]); b) DC sheet resistance vs transmittance at 550 nm for SWNT films of various densities (from Li et al., [130]) ; c) Transmission of a P3HT wrapped SWNT nanohybrid layer compared to a PEDOT/PSS film, and d) AFM image of the nanohybrid SWNT network (from Dabera et al., [131]). e) J-V characteristics of OPV devices with either SWNT or ITO electrodes, and with and without PEDOT as an HTL. Solid lines represent current under simulated solar light, and dashed curves are dark current. Inset: NREL-certified light J-V data for devices with a SWNT electrode only (from Barnes et al., [122]).

tance of 300 Ω / □ with 96.4% transparency. [137] Moreover, recently P3HT wrapped s-SWNT thin films (≈10-20 nm) were used as hole extraction layers, and provided similar, or slightly better, transmittance as poly(3,4-ethylenedioxythiophene)/poly (styrene sulfonate) (PEDOT/PSS) films spun on ITO (Figure 8 c,d). [131]

Roll-to-roll fabrication of SWNT electrodes has been shown, and flexible OLEDs and OPVs have been reported, with efficiencies comparable to devices made with ITO electrodes. [10] The use of nanotubes as charge collectors has also been demonstrated with PV technologies based on inorganic thin films. Contreras et al. used a SWNT network to replace the ZnO transparent oxide in copper indium gallium selenide (CIGS) solar cells, achieving a power conversion efficiency (PCE) of sunlight to electricity of 13 % [138]. Similarly, Barnes et al. used a SWNT layer as a semi-transparent back contact in cadmium telluride (CdTe) solar cells, demonstrating a PCE of 12.4 % [139]. Carbon nanotubes have also been shown to perform respectably as transparent electrodes in silicon-based photovoltaics [140], dye-sensitized solar cells [141], and as conducting scaffolds in TiO_2-based photoelectrochemical cells [142].

4.2 Organic Photovoltaic (OPV) Devices

The operation of an organic photovoltaic (OPV) device typically involves photo-generation of a bound electron-hole pair (exciton), which is then dissociated at a heterojunction and the separated electron and hole then transported to opposite electrodes. State-of-the-art OPV devices incorporate low bandgap polymer absorbers and fullerene-like electron acceptors, with power conversion efficiencies (PCEs) now exceeding 10 % [143]. However, the favorable properties of SWNTs may enable them to be integrated into OPVs to further improve performance [32]. SWNTS can play three possible roles in the photoactive layer of OPV devices: as electron acceptors, as hole acceptors or as the light-harvesting donor material. An excellent review of the photophysics of carbon nanotubes for these applications is given by Arnold et al. [31]. We summarise selected

works using carbon nanotubes in the active layers of photovoltaics in Table 2.

Nanotubes have been incorporated into OPV devices as hole acceptors either by tuning the nanotube Fermi level [82] or by blending SWNTs with fullerenes, which have a larger electron affinity. These devices demonstrated increased efficiencies (3.7 %) compared to those without nanotubes (3.1 %), which was attributed to increased hole mobilities and enhanced exciton dissociation. [144, 145] Much of the early work focused on the use of SWNTs as the electron acceptor material by directly replacing the fullerene (PCBM) in polymer devices. These studies typically utilized mixtures of large-diameter semiconducting and metallic arc-discharge SWNTs blended with polythiophene polymers similar to P3HT, namely poly(3-octylthiophene) (P3OT), where the hexyl side chains are replaced with octyl chains. Performances were low (η <0.1 %) but peculiarly high V_{OC} values of 0.7–1 V were observed. [146–149] These values were far higher than the predicted values from the energy level differences, suggesting that a different model may be required to describe the OPV blends which incorporate SWNTs. Similarly poor device efficiencies (η =0.22 %) were obtained using blends with larger bandgap polymers such as poly(2-methoxy-5-(2-ethylhexyloxy)-1,4-phenylenevinylene) (MEHPPV) or crystallized polyfluorenes. [150–152]

The low observed efficiencies in nanotube-polymer blends can be explained by recent theoretical [160] and experimental work [53] showing that the required type-II heterojunction only forms between P3HT and *small-diameter, semiconducting* nanotubes (see Section 2.3). In these cases, the driving forces for exciton dissociation (ΔG_0 ~1.2 eV) even exceed that for PCBM as the acceptor material (~0.9 eV) [161]. Metallic nanotubes are also detrimental to device performance by acting as efficient recombination centers, quenching both excitons and free charges [37, 162]. Most of the early work utilized large-diameter nanotubes with mixtures of both metallic and semiconducting species, which only form type-I heterojunction alignments, and unwanted energy transfer is the dominant process over exciton dissociation. Moreover,

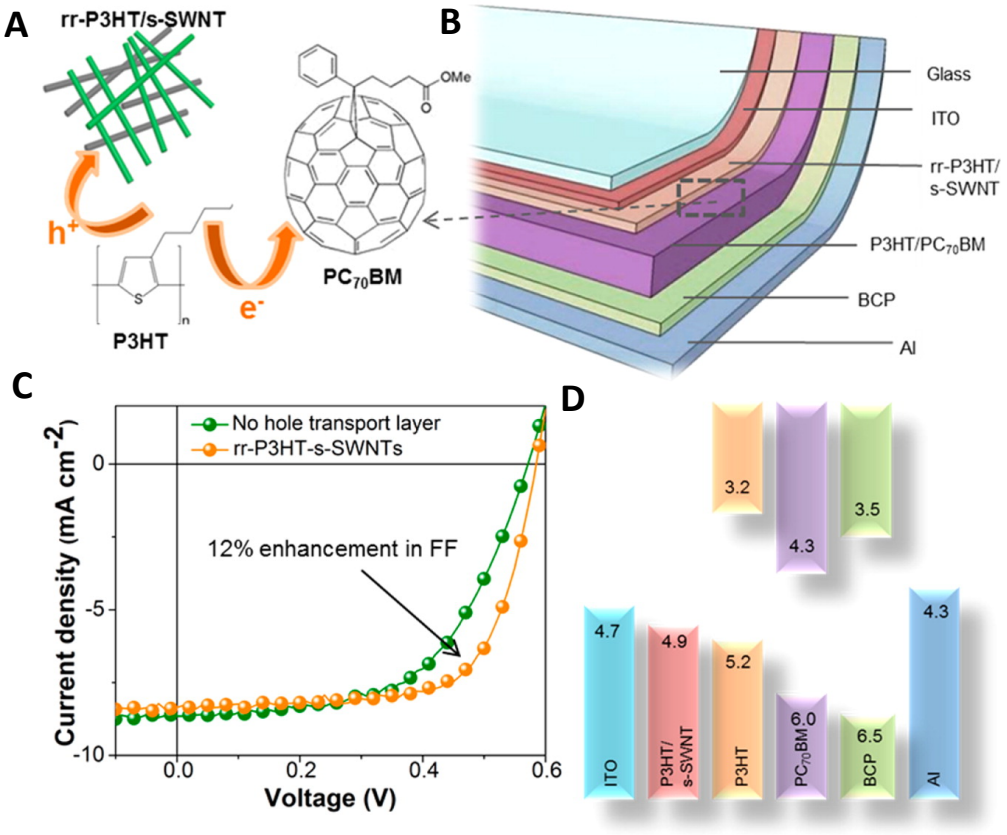

Figure 9: Demonstration of polymer wrapped P3HT-SWNTs nanohybrids as hole transport layer in an OPV device. a) Charge transfer at the interface between P3HT and PCBM in a photovoltaic device, using regio-regular rr-P3HT wrapped SWNTs which serve as hole transport layer. b) Schematic representation of the OPV device architecture with the P3HT-SWNTs nanohybrids HTL. c) J-V characteristics of devices with and without P3HT-SWNTs HTL under AM 1.5G illumination and 100 mW cm^{-2} irradiance. d) Energy band diagram (in eV) for the device shown in (b). From Dabera et al., [131].

Group	Year	Architecture (Nanotube source)	η (%)
Nanotubes as hole acceptors in OPV			
Chaudhary *et al.* [144]	2007	ITO/PEDOT:PSS/SWNT(HiPCO)/P3HT:PCBM/Al	3.7
Bindl *et al.* [153]	2011	ITO/sSWNT(HiPCO)-PFO/C60/BCP/Ag	0.6
Kymakis *et al.* [145]	2012	ITO/SWNT(arc)/P3HT:PCBM/Al	3
Dabera *et al.* [131]	2012	ITO/sSWNT(HiPCO)-P3HT/PTB7-PCBM/BCP/Al	7.6
Nanotubes as electron acceptors in OPV			
Kymakis *et al.* [147]	2003	ITO/P3OT-SWNT(arc)/Al	0.06
Kazaoui *et al.* [150]	2005	ITO/P3OT-SWNT(HiPCO)/Al	0.1
		ITO/MEHPPV-SWNT(HiPCO)/Al	0.001
Kymakis *et al.* [151]	2006	ITO/PEDOT:PSS/P3OT-SWNT(arc)/Al	0.2
Ren *et al.* [154]	2012	ITO/PEDOT:PSS/P3HT-sSWNT(HiPCO)/BCP/Al	0.7
Nanotubes as light-harvesting materials in OPV			
Shea and Arnold [155]	2013	ITO/PFO-sSWNT(CoMoCAT)/C60/BCP/Ag	0.95
Gong et al. [156]	2014	ITO/ZnO/PFO-sSWNT(HiPCO)/MoOx/Ag	3.1
Nanotubes as hole transporters in perovskite solar cells			
Habisreutinger et al. [157]	2014	FTO/TiO_2/Al_2O_3-$MAPbI_3$/ P3HT-mSWNT(CoMoCAT)-PMMA/Ag	15.3
Habisreutinger et al. [158]	2014	FTO/TiO_2/Al_2O_3-$MAPbI_3$/ P3HT-mSWNT(CoMoCAT)/Spiro-OMeTAD/Ag	15.4
Aitola et al. [159]	2016	FTO/TiO_2/(MA/FA)$Pb(I/Br)_3$/ SWNT(CVD)/Spiro-OMeTAD/Ag	15.5

Table 2: Summary of progress in the field of OPV devices utilising carbon nanotube–polymer blends. The list is not exhaustive but summarises key progressions over time. All tabulated results were recorded under simulated solar light (100 mW/cm^2, AM 1.5). Arc refers to arc-discharge and CVD to chemical vapor deposition nanotube synthesis, the s or m prefix on SWNT denotes semiconducting- or metallic-enriched distributions, respectively, obtained as starting material or enriched through selective polymer-dispersion, PEDOT:PSS (poly(3,4-ethylenedioxythiophene) polystyrene sulfonate), BCP (bathocuproine), MA - methylammonium, FA - formamidinium

the polymer-nanotube blend structures were not well characterized, leading to sub-optimal interfaces and morphologies. Recently, the use of SWNTs as a transport layer was demonstrated for organic and hybrid optoelectronic devices. Due to their high work function (4.9 eV), SWNTs can efficiently inject or extract holes in OPVs and organic LEDs (OLEDs), and OPV devices using SWNT electrodes resulted in similar or better J-V characteristics and efficiencies compared to electrodes made of ITO, and ITO covered by PEDOT/PSS (Figure 8 e). [122, 163] Polymer wrapped P3HT-SWNTs nanohybrids acting as hole transport layer deposited on ITO/glass have been integrated into a P3HT/PCBM bulk heterojunction OPV device [131] (**Figure 9 a,b**), resulting in a 12% increased fill factor and overall device efficiency (Figure 9 c,d).

The work presented in Section 2.3 (Figure 4) suggests that efficient devices utilizing nanotubes as the electron acceptors will require the use of well-optimized nanotube-polymer structures, where the nanotube components are only present in small percentages and purely as small-diameter, semiconducting tubes. As an encouraging validation, Ren *et al.* incorporated nanofilaments comprised of small-diameter, semiconducting nanotubes coated with P3HT polymer into OPV devices, observing a PCE of 0.73 % with a nanotube weight percentage of 3 % [154] (Figure 10a). A recent study also reported on the advantages of using purely s-SWNTs in small quantities (0.02-0.04 wt%), showing improved PCE efficiencies above 6% in a PTB7/PCBM solar cell. [164] This work also showed the importance of good SWNT dispersion and network formation at low tube loading using a N-Methyl-2-pyrrolidone (NMP) dispersant.

A particularly attractive OPV device concept utilizes SWNTs as the light-harvesting material, with exciton dissociation and electron transfer to a fullerene-based acceptor. [153, 165] A key advantage of this approach is that the nanotubes absorb strongly in the near-infrared, therefore enabling the harnessing of a portion of the solar spectrum that is currently inaccessible to many other thin film PV technologies. In these first attempts, the authors used the PFO sorting route described in Section 2.1 to yield a

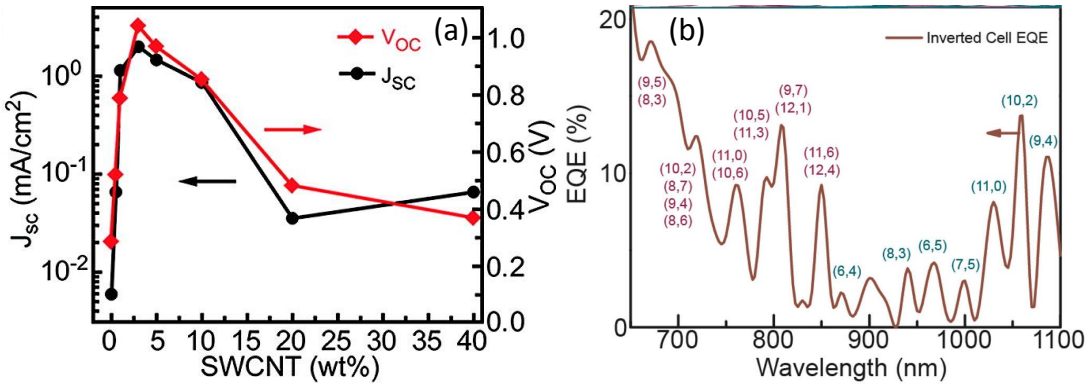

Figure 10: Carbon Nanotube-based OPVs. (a) The open-circuit voltage (red curve) and short-circuit current (black curve) as a function of the SWNT weight fraction in the active layer for P3HT/s-SWCNT nanofilament based solar cells. From Ren et al. [154]. (b) Near-IR external quantum efficiency (EQE) of a polychiral CNT-based OPV device plotted with the SWCNT chiral distribution, where there is strong overlap between the EQE and the absorption of each tube. From Gong et al. [156].

monochiral dispersion and achieved a PCE of ∼1 %, with an external quantum efficiency (EQE) of 43 % at the nanotube bandgap. [155] However, the EQEs were only significant at the sharp van Hove singularities of the nanotubes, and hence only a fraction of the solar spectrum could be harvested. Hersam and co-workers recently broadened the light harvesting ability by utilizing a polychiral distribution of semiconducting SWNTs (Figure 10b), leading to average certified and champion PCEs of 2.5 % and 3.1 %, respectively [156]. Further improvements could be made by using novel bulk heterojunction approaches. [166] A recent spectroscopic study by Ihly et al. revealed that there can be a very strong driving force for efficient photoinduced electron transfer between SWNTs and particular fullerene derivatives, suggesting that further improvements to these systems could also be achieved by judicious choice of fullerene derivatives. [167]

4.3 Carbon Nanotubes in Perovskite Solar Cells

Organic-inorganic perovskites such as $CH_3NH_3PbI_3$ have rapidly emerged as serious contenders to rival the leading PV technologies, where PCEs have sky-rocketed from

3 % to over 20 % in just three years of academic research. [168] The properties of these perovskites which have enabled highly efficient devices include a strong absorption coefficient with sharp absorption edge [169], low levels of non-radiative decay loss (i.e. high emission quantum efficiency) [170], high fractions of free charge due to low exciton binding energies [171], and charge carrier diffusion lengths on the order of microns [172]. The tunability of bandgap by tuning the components of the ABX_3 perovskite crystal structure (Figure 11(a) and ease of processing using a range of deposition methods onto any desired substrates (eg. rigid or flexible) lends them to application in a variety of colorful and novel PV and light-emitting devices. [168] Typical PV devices have a PCE of $\sim$15 % and consist of a thin perovskite layer sandwiched between n- and p-type contacts, in a n-i-p architecture. The perovskite absorbs the incident light, generates free electrons and holes, and transports these charges to the respective contacts. Although we have witnessed rapid improvements in PCE, a number of challenges remain before we will see commercialization of the perovskite technology. One of the most pressing is that the workhorse perovskite materials ($CH_3NH_3PbI_3$) and charge collection layers are unstable and will degrade rapidly if exposed to moisture and/or high temperature. [168, 173]

A particularly promising application of SWNT networks is as the transparent hole transporting material (HTM) in perovskite solar cells. One of us and co-workers recently proposed one elegant solution to the stability issue, where we replaced the standard HTM Spiro-OMeTAD with P3HT-wrapped SWNTs embedded in an insulating polymer matrix (Figure 11(b)). [157, 158] We observed a PCE of up to 15.3 %, which is comparable to those with the standard Spiro-OMeTAD as the HTM, but we also observed a strong retardation in thermal degradation and enhanced resistance to water ingress in the CNT system when compared to the standard HTMs, with a device even directly exposed to running water for extended periods showing very little drop in performance. The concept of a carbon-based encapsulating layer is promising; Mei et

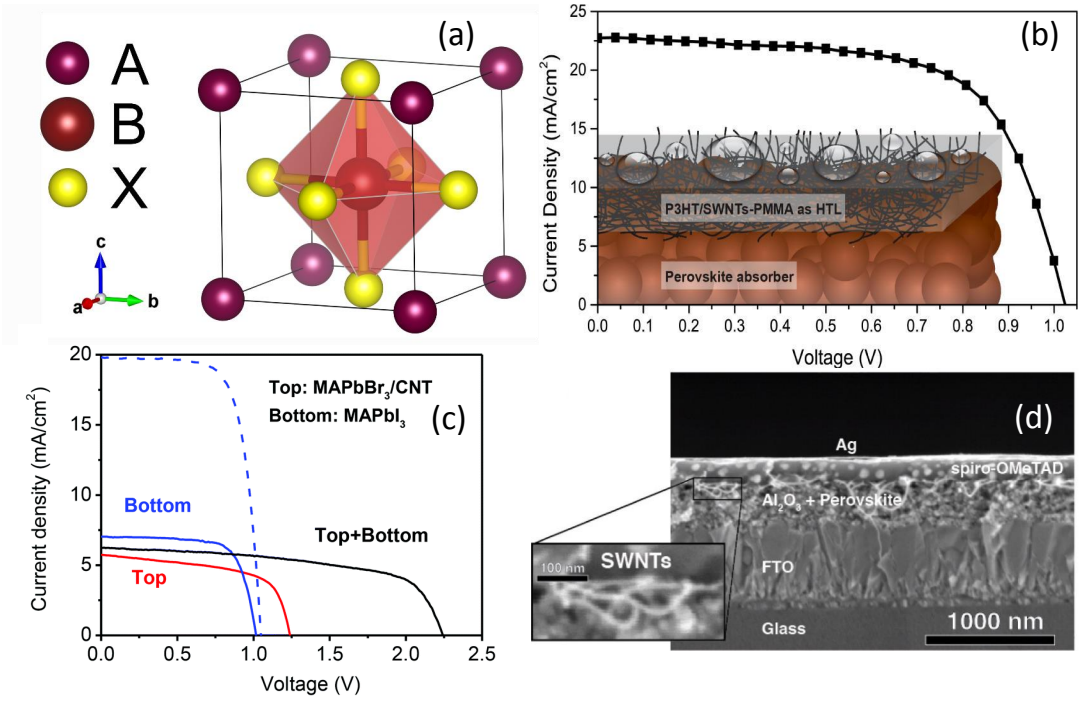

Figure 11: Carbon Nanotubes in Perovskite PV. (a) Perovskite crystal structure, where hybrid perovskites typically have A=CH_3NH_3, B=Pb, X=I, Br or Cl. (d) Current-voltage curve of a perovksite solar cell incorporating [P3HT-NT] nanohybrids in a PMMA matrix as the hole transporting material. A cartoon of the device structure is shown in the inset. From Habisreutinger et al. [157]. (c) Light JV curves of a tandem solar cell formed by stacking a transparent $MAPbBr_3$/CNT (top) solar cell and a $MAPbI_3$ (bottom) solar cell and connected in series. The dash curves represent the $MAPbI_3$ solar cell before stacking. From Li et al. [174] (d) Cross-section SEM image of a device with a blend structure composed of undoped spiro-OMeTAD and P3HT/SWNTs. Individual SWNTs can be seen to protrude from the interface between the alumina scaffold and spiro-OMeTAD layers. From Habisreutinger et al. [158]

al. [175] recently demonstrated that a device fabricated by infiltrating the perovskite into a thick porous carbon film exhibits excellent stability even during outdoor testing under full sunlight. [176]

Several groups have reported that Spiro-OMeTAD HTM could also be improved with the incorporation of SWNTs [158, 159, 177] either as a blend or in a stratified structure (Figure 11(d)), with PCEs reaching over 15 %. These combined CNT/Spiro-OMeTAD HTMs could even be contacted directly and maintain good device performance without the need for an additional top metal electrode; this was also possible with CNTs alone though with inferior performance to the combined CNT/Spiro-OMeTAD analogues. [159, 177] These results demonstrate the enormous potential for using CNTs as transparent top electrodes in perovskite solar cells. Li et al. demonstrated that this concept could be employed in a perovskite-perovskite tandem solar cell connected in series, where a large bandgap $MAPbBr_3$ perovskite top device incorporating a transparent CNT top electrode absorbs the high energy light but allows the lower energy light to pass through to the bottom cell where the light is absorbed by the lower bandgap $MAPbI_3$ perovskite. [174] Although the overall efficiency did not improve on this first demonstration, the additive nature of the open-circuit voltage to 2.24 V is highly encouraging (Figure 11(c)).

Cai et al. showed that they could also get substantial PCE improvements when incorporating low fractions of CNTs into a P3HT HTM [178], which are similar findings to those of Ren et al. [154] for OPV. Wang et al. constructed a fully-flexible perovskite PV device with a PCE of 8.3 % using electron-collecting TiO_2 nanotubes on a metal foil as flexible substrate and a CNT network as the transparent HTM. [179] In the 'inverted' p-i-n perovskite solar cell architecture, Jeon et al. were able to replace ITO on the glass substrate with SWNTs and still retain reasonable performance. [180] This is an important step for future low-cost scalability of this particular device architecture.

The efficient hole collecting properties of the SWNT from the perovskite was re-

cently explained by Schulz et al. [181] They found that a ground state electron transfer from the $MAPbI_3$ perovskite to the SWNT makes the SWNT n-type at the interface. This establishes a band bending that is favorable for efficient photo-excited hole transfer from $MAPbI_3$ to SWNT but with a barrier for any hole transfer back to the $MAPbI_3$.

5 Future directions and challenges

Carbon nanotubes have a variety of properties that make them ideal for optoelectronic applications. Nevertheless, they have not yet reached their full potential and thus we are yet to see carbon nanotube optoelectronics seriously approaching commercialization. While their aspect ratios and properties such as chirality can be exploited advantageously, these very same properties also make them challenging to work with due to the the polydispersity in both chirality and electronic nature (semiconducting or metallic) and their tendency to form bundles. The difficulty to control synthesis to prevent these undesired phenomena has seriously hindered optoelectronic development, and this has seen them largely overlooked for device implementation to date in favor of their allotropic cousins fullerenes (0D) and graphene (2D). The most fundamental challenge is to find ways to controllably and scalably synthesize high quality single chirality nanotubes. Recent work by Sanchez-Valencia et al. [42], where the authors controllably synthesise nearly defect-free (6,6) nanotubes, is highly encouraging. Further work will be needed to synthesize other chiralities and to demonstrate scalability. Other techniques such as selective polymer wrapping and subsequent polymer exchange to form customized heterojunctions are also highly encouraging [58, 59] though scalability will need to be shown.

Nevertheless, controlled carbon nanotube nano-networks and polymer nano-hybrids show tremendous promise for use in a variety of applications including photovoltaics. The favorable absorptions of nano-hybrids in the visible and near-infrared could lead to

very efficient harvesting of the solar spectrum [156], which could be further enhanced with polymer-wrapped sensitizers [58]. Using these structures as the active components in solar cells continues to be a tantalizing prospect. The prototypes to date all exploit random networks of nanotubes, which are not ideal due to the formation of aggregates and sub-optimal tube interconnections. The nanoscale architecture of the networks is an important factor to further enhance charge transport. The controlled formation of networks in nanoscale domains described in Section 3.3 could therefore be a compelling strategy to further increase PV device efficiencies, and reduce nanotube loading. For example, solution-processed nanoscale SWNT networks were engineered in a P3HT film and led to an enhancement in charge transport by 2-orders-of-magnitude at very low tube concentrations (<0.1 wt%) compared to a random network. [119]

Finally, one of the most exciting new fields in PV is perovskite solar cells, and we will expect to see many more reports integrating CNTs into these systems over the coming years as the field rapidly evolves. The CNTs are likely to be particularly advantageous as charge collection layers, with encouraging first examples given in Section 4.3. CNT-based transport layers could be more stable and superior to the existing extraction layers; indeed, recent reports have suggested that adoption of stable alternatives could be the key to improved perovskite device performance and long-term operational stability. [173]

A first application for this promising perovskite technology is likely to be in hybrid tandems with crystalline silicon (c-Si) as an additional active absorbing layer to further improve the efficiency of the state-of-the-art silicon solar cells. [182] Incremental improvements in the PCE of c-Si solar cells to and beyond its current value of 25 % has been slow due to the maturity of the technology, but it is estimated that incorporation of a top perovskite layer could theoretically increase the PCE to 35 % [183], which would substantially lower the cost of PV. These hybrid tandems require a transparent top electrode on the perovskite. The first embodiments utilized silver nanowires for

these electrodes [184, 185], but carbon nanotube networks could be a very promising alternative. Moreover, the perovskite processing tunability has enabled the realization of efficient semi-transparent devices [186, 187], and carbon nanotubes could also act as efficient top contacts [174]. These devices could find widespread application in building-integrated PV, as one example.

By clever manipulation of nanotubes and networks on the nanoscale, we may be able to truly unlock the variety of oustanding properties promised by carbon nanotubes, leading to widespread adoption of the materials in a multitude of applications. One day, we may see carbon nanotubes and their allotropic cousins graphene and fullerenes power and light the world through carbon-based solar cells, batteries, displays, light-emitting diodes and lasers.

Acknowledgements

The authors acknowledge financial support from the Baltic Foundation, the Kempe Foundation, and the People Programme (Marie Curie Actions) of the European Union's Seventh Framework Programme (FP7/2007-2013) under REA grant agreement number PIOF-GA-2013-622630 D. R. B. would also like to thank a Young Researcher Career Award at Umeå University for support of this work. S.D.S. acknowledges Richard H. Friend and Vladimir Bulović for additional support.

References

[1] M. Treacy, T. Ebbesen, J. Gibson, *Nature* **1996**.

[2] A. Krishnan, E. Dujardin, T. Ebbesen, P. Yianilos, M. Treacy, *Physical Review B* **1998**, *58*(20), 14013.

[3] M. Falvo, G. Clary, R. Taylor, V. Chi, F. Brooks, S. Washburn, R. Superfine, *Nature* **1997**, *389*(6651), 582–584.

[4] E. W. Wong, P. E. Sheehan, C. M. Lieber, *Science* **1997**, *277*(5334), 1971–1975.

[5] L. Jin, C. Bower, O. Zhou, *Applied physics letters* **1998**, *73*(9), 1197–1199.

[6] R. Haggenmueller, H. Gommans, A. Rinzler, J. E. Fischer, K. Winey, *Chemical physics letters* **2000**, *330*(3), 219–225.

[7] E. Artukovic, M. Kaempgen, D. Hecht, S. Roth, G. Grüner, *Nano Letters* **2005**, *5*(4), 757–760.

[8] M. Kaempgen, C. K. Chan, J. Ma, Y. Cui, G. Gruner, *Nano letters* **2009**, *9*(5), 1872–1876.

[9] G. Gruner, *J. Mater. Chem.* **2006**, *16*(35), 3533–3539.

[10] M. W. Rowell, M. A. Topinka, M. D. McGehee, H.-J. Prall, G. Dennler, N. S. Sariciftci, L. Hu, G. Gruner, *Applied Physics Letters* **2006**, *88*(23), 233506.

[11] S. Hong, S. Myung, *Nature Nanotechnology* **2007**, *2*(4), 207–208.

[12] D. Zhang, K. Ryu, X. Liu, E. Polikarpov, J. Ly, M. E. Tompson, C. Zhou, *Nano Letters* **2006**, *6*(9), 1880–1886.

[13] S. Iijima, T. Ichihashi, *Nature* **1993**.

[14] D. Bethune, C. Klang, M. De Vries, G. Gorman, R. Savoy, J. Vazquez, R. Beyers, *Nature* **1993**.

[15] M. Dresselhaus, G. Dresselhaus, R. Saito, *Carbon* **1995**, *33*(7), 883–891.

[16] J. Kong, E. Yenilmez, T. W. Tombler, W. Kim, H. Dai, R. B. Laughlin, L. Liu, C. Jayanthi, S. Wu, *Physical review letters* **2001**, *87*(10), 106801.

[17] W. Liang, M. Bockrath, D. Bozovic, J. H. Hafner, M. Tinkham, H. Park, *Nature* **2001**, *411*(6838), 665–669.

[18] D. Mann, A. Javey, J. Kong, Q. Wang, H. Dai, *Nano Letters* **2003**, *3*(11), 1541–1544.

[19] A. Bachtold, M. Fuhrer, S. Plyasunov, M. Forero, E. H. Anderson, A. Zettl, P. L. McEuen, *Physical Review Letters* **2000**, *84*(26), 6082.

[20] P. L. McEuen, M. S. Fuhrer, H. Park, *IEEE transactions on nanotechnology* **2002**, *1*(1), 78–85.

[21] S. J. Tans, A. R. Verschueren, C. Dekker, *Nature* **1998**, *393*(6680), 49–52.

[22] M. S. Arnold, J. D. Zimmerman, C. K. Renshaw, X. Xu, R. R. Lunt, C. M. Austin, S. R. Forrest, *Nano Lett.* **2009**, *9*(9), 3354–3358.

[23] P.-L. Ong, W. B. Euler, I. A. Levitsky, *Nanotechnology* **2010**, *21*, 105203.

[24] J. Wei, Y. Jia, Q. Shu, Z. Gu, K. Wang, D. Zhuang, G. Zhang, Z. Wang, J. Luo, A. Cao, D. Wu, *Nano Lett.* **2007**, *7*(8), 2317–2321.

[25] S. Ren, M. Bernardi, R. R. Lunt, V. Bulovic, J. C. Grossman, S. Gradecak, *Nano Lett.* **2011**, *11*(12), 5316–5321.

[26] Y. Imai, C. E. Finlayson, P. Goldberg-Oppenheimer, Q. Zhao, P. Spahn, D. R. E. Snoswell, A. I. Haines, G. P. Hellmann, J. J. Baumberg, *Soft Matter* **2012**, *8*, 6280–6290.

[27] M. Bernardi, J. Lohrman, P. V. Kumar, A. Kirkeminde, N. Ferralis, J. C. Grossman, S. Ren, *ACS Nano* **2012**, *6*(10), 8896–8903.

[28] E. Miyako, H. Nagata, K. Hirano, T. Hirotsu, *Adv. Mater.* **2009**, *21*, 2819–2823.

[29] E. Kymakis, M. M. Stylianakis, G. D. Spyropoulos, E. Stratakis, E. Koudoumas, C. Fotakis, *Sol. Energy Mater. Sol. Cells* **2012**, *96*, 298–301.

[30] Z. Yang, T. Chen, R. He, G. Guan, H. Li, L. Qiu, H. Peng, *Adv. Mater.* **2011**, *23*(45), 5436–5439.

[31] M. S. Arnold, J. L. Blackburn, J. J. Crochet, S. K. Doorn, J. G. Duque, A. Mohite, H. Telg, *Phys. Chem. Chem. Phys.* **2013**, *15*, 14896–14918.

[32] S. Cataldo, P. Salice, E. Menna, B. Pignataro, *Energy Environ. Sci.* **2012**, *5*, 5919–5940.

[33] S. Chopra, K. McGuire, N. Gothard, A. Rao, A. Pham, *Applied Physics Letters* **2003**, *83*(11), 2280–2282.

[34] J. Li, Y. Lu, Q. Ye, M. Cinke, J. Han, M. Meyyappan, *Nano Letters* **2003**, *3*(7), 929–933.

[35] S. D. Stranks, Ph.D. thesis, University of Oxford **2011**.

[36] X. Zhou, J.-Y. Park, S. Huang, J. Liu, P. L. McEuen, *Physical Review Letters* **2005**, *95*(14), 146805.

[37] J. M. Holt, A. J. Ferguson, N. Kopidakis, B. A. Larsen, J. Bult, G. Rumbles, J. L. Blackburn, *Nano Lett.* **2010**, *10*, 4627 – 4633.

[38] H. P. Liu, D. Nishide, T. Tanaka, H. Kataura, *Nat. Commun.* **2011**, *2*, 309.

[39] M. S. Arnold, A. A. Green, J. F. Hulvat, S. I. Stupp, M. C. Hersam, *Nat. Nanotechnol.* **2006**, *1*, 60–65.

[40] J. Liu, C. Wang, X. Tu, B. Liu, L. Chen, M. Zheng, C. Zhou, *Nature Communications* **2012**, *3*, 1199.

[41] F. Yang, X. Wang, D. Zhang, J. Yang, D. Luo, Z. Xu, J. Wei, J.-Q. Wang, Z. Xu, F. Peng, et al., *Nature* **2014**, *510*(7506), 522–524.

[42] J. R. Sanchez-Valencia, T. Dienel, O. Groning, I. Shorubalko, A. Mueller, M. Jansen, K. Amsharov, P. Ruffieux, R. Fasel, *Nature* **2014**, *512*, 61–64.

[43] J. L. Bahr, E. T. Mickelson, M. J. Bronikowski, R. E. Smalley, J. M. Tour, *Chem. Commun.* **2001**, *2*, 193 – 194.

[44] S. D. Bergin, Z. Sun, P. Streich, J. Hamilton, J. N. Coleman, *The Journal of Physical Chemistry C* **2010**, *114*(1), 231–237.

[45] S. S. Wong, E. Joselevich, A. T. Woolley, C. L. Cheung, C. M. Lieber, *Nature* **1998**, *394*(6688), 52–55.

[46] J. L. Bahr, J. Yang, D. V. Kosynkin, M. J. Bronikowski, R. E. Smalley, J. M. Tour, *Journal of the American Chemical Society* **2001**, *123*(27), 6536–6542.

[47] P. K. Rai, R. A. Pinnick, A. N. G. Parra-Vasquez, V. A. Davis, H. K. Schmidt, R. H. Hauge, R. E. Smalley, M. Pasquali, *Journal of the American Chemical Society* **2006**, *128*(2), 591–595.

[48] V. Skakalova, A. Kaiser, U. Dettlaff-Weglikowska, K. Hrncarikova, S. Roth, *The Journal of Physical Chemistry B* **2005**, *109*(15), 7174–7181.

[49] M. Deborah, A. Jawahar, T. Mathavan, M. K. Dhas, A. M. F. Benial, *Spectrochimica Acta Part A: Molecular and Biomolecular Spectroscopy* **2014**.

[50] M. J. O'Connell, S. M. Bachilo, C. B. Huffman, V. C. Moore, M. S. Strano, E. H. Haroz, K. L. Rialon, P. J. Boul, W. H. Noon, C. Kittrell, J. P. Ma, R. H. Hauge, R. B. Weisman, R. E. Smalley, *Science* **2002**, *297*, 593–596.

[51] S. Reich, C. Thomsen, J. Maultzsch, *Carbon Nanotubes – Basic Concepts and Physical Properties*, Wiley-VCH, first edition **2004**.

[52] R. B. Weisman, S. M. Bachilo, *Nano Lett.* **2003**, *3*, 1235 – 1238.

[53] T. Schuettfort, A. Nish, R. J. Nicholas, *Nano Lett.* **2009**, *9*, 3871 – 3876.

[54] M. J. O'Connell, P. Boul, L. M. Ericson, C. Huffman, Y. H. Wang, E. Haroz, C. Kuper, J. Tour, K. D. Ausman, R. E. Smalley, *Chem. Phys. Lett.* **2001**, *342*, 265–271.

[55] A. Nish, J. Y. Hwang, J. Doig, R. J. Nicholas, *Nat. Nanotechnol.* **2007**, *2*, 640 – 646.

[56] J. Y. Hwang, A. Nish, J. Doig, S. Douven, C.-W. Chen, L. C. Chen, R. J. Nicholas, *J. Am. Chem. Soc.* **2008**, *130*, 3543–3553.

[57] T. Schuettfort, H. Snaith, A. Nish, R. Nicholas, *Nanotechnology* **2010**, *21*, 025201.

[58] S. D. Stranks, A. M. R. Baker, J. A. Alexander-Webber, B. Dirks, R. J. Nicholas, *Small* **2013**, *9*, 2245–2249.

[59] S. D. Stranks, S. N. Habisreutinger, B. Dirks, R. J. Nicholas, *Advanced Materials* **2013**, *25*, 4365–4371.

[60] D. Tuncel, *Nanoscale* **2011**, *3*, 3545–3554.

[61] F. Toshimitsu, N. Nakashima, *Nat Commun* **2014**, *5*, 5041.

[62] V. Derycke, R. Martel, J. Appenzeller, P. Avouris, *Nano Letters* **2001**, *1*(9), 453–456.

[63] J. O. Hwang, J. S. Park, D. S. Choi, J. Y. Kim, S. H. Lee, K. E. Lee, Y.-H. Kim, M. H. Song, S. Yoo, S. O. Kim, *Acs Nano* **2011**, *6*(1), 159–167.

[64] J. Kong, N. R. Franklin, C. Zhou, M. G. Chapline, S. Peng, K. Cho, H. Dai, *science* **2000**, *287*(5453), 622–625.

[65] V. Derycke, R. Martel, J. Appenzeller, P. Avouris, *Applied Physics Letters* **2002**, *80*(15), 2773–2775.

[66] R. J. Chen, N. R. Franklin, J. Kong, J. Cao, T. W. Tombler, Y. Zhang, H. Dai, *Applied Physics Letters* **2001**, *79*(14), 2258–2260.

[67] M. Bockrath, J. Hone, A. Zettl, P. L. McEuen, A. G. Rinzler, R. E. Smalley, *Physical Review B* **2000**, *61*(16), R10606.

[68] T. Takenobu, T. Takano, M. Shiraishi, Y. Murakami, M. Ata, H. Kataura, Y. Achiba, Y. Iwasa, *Nature materials* **2003**, *2*(10), 683–688.

[69] Y. Lu, W. Chen, Y. Feng, P. He, *The Journal of Physical Chemistry B* **2008**, *113*(1), 2–5.

[70] X. Dong, D. Fu, W. Fang, Y. Shi, P. Chen, L.-J. Li, *Small* **2009**, *5*(12), 1422–1426.

[71] Y. Nonoguchi, K. Ohashi, R. Kanazawa, K. Ashiba, K. Hata, T. Nakagawa, C. Adachi, T. Tanase, T. Kawai, *Scientific reports* **2013**, *3*.

[72] M. Shim, A. Javey, N. W. Shi Kam, H. Dai, *Journal of the American Chemical Society* **2001**, *123*(46), 11512–11513.

[73] J. Zhu, B. S. Shim, M. Di Prima, N. A. Kotov, *Journal of the American Chemical Society* **2011**, *133*(19), 7450–7460.

[74] W. Z. Yuan, J. Z. Sun, Y. Dong, M. Häussler, F. Yang, H. P. Xu, A. Qin, J. W. Lam, Q. Zheng, B. Z. Tang, *Macromolecules* **2006**, *39*(23), 8011–8020.

[75] M. A. Herranz, C. Ehli, S. Campidelli, M. Gutiérrez, G. L. Hug, K. Ohkubo, S. Fukuzumi, M. Prato, N. Martín, D. M. Guldi, *Journal of the American Chemical Society* **2008**, *130*(1), 66–73.

[76] S. D. Stranks, C.-K. Yong, J. A. Alexander-Webber, C. Weisspfennig, M. B. Johnston, L. M. Herz, R. J. Nicholas, *ACS nano* **2012**, *6*(7), 6058–6066.

[77] S. D. Stranks, C. Weisspfennig, P. Parkinson, M. B. Johnston, L. M. Herz, R. J. Nicholas, *Nano Lett.* **2011**, *11*, 66 – 72.

[78] J.-Y. Hwang, A. Nish, J. Doig, S. Douven, C.-W. Chen, L.-C. Chen, , R. J. Nicholas, *Journal of the American Chemical Society* **2008**, *130*(11), 3543–3553, pMID: 18293976.

[79] H. W. Lee, Y. Yoon, S. Park, J. H. Oh, S. Hong, L. S. Liyanage, H. Wang, S. Morishita, N. Patil, Y. J. Park, J. J. Park, A. Spakowitz, G. Galli, F. Gygi, P. H. S. Wong, J. B. H. Tok, J. M. Kim, Z. Bao, *Nat Commun* **2011**, *2*, 541.

[80] P. Gerstel, S. Klumpp, F. Hennrich, O. Altintas, T. R. Eaton, M. Mayor, C. Barner-Kowollik, M. M. Kappes, *Polymer Chemistry* **2012**, *3*(8), 1966–1970.

[81] Y. Kanai, J. C. Grossman, *Nano letters* **2007**, *7*(7), 1967–1972.

[82] N. M. Dissanayake, Z. Zhong, *Nano letters* **2010**, *11*(1), 286–290.

[83] M. Bernardi, M. Giulianini, J. C. Grossman, *ACS nano* **2010**, *4*(11), 6599–6606.

[84] I. Robel, B. Bunker, P. Kamat, *Advanced Materials* **2005**, *17*(20), 2458–2463.

[85] S. D. Stranks, C.-K. Yong, J. A. Alexander-Webber, C. Weisspfennig, M. B. Johnston, L. M. Herz, R. J. Nicholas, *ACS Nano* **2012**, *6*(7), 6058–6066.

[86] A. V. Kyrylyuk, P. van der Schoot, *Proceedings of the National Academy of Sciences* **2008**, *105*(24), 8221–8226.

[87] S. Z. Bisri, J. Gao, V. Derenskyi, W. Gomulya, I. Iezhokin, P. Gordiichuk, A. Herrmann, M. A. Loi, *Advanced Materials* **2012**, *24*(46), 6147–6152.

[88] I. Balberg, C. Anderson, S. Alexander, N. Wagner, *Physical review B* **1984**, *30*(7), 3933.

[89] I. Balberg, N. Binenbaum, N. Wagner, *Physical Review Letters* **1984**, *52*(17), 1465.

[90] I. Balberg, *Physical review B* **1985**, *31*(6), 4053.

[91] L. Onsager, *Annals of the New York Academy of Sciences* **1949**, *51*(4), 627–659.

[92] M. Foygel, R. Morris, D. Anez, S. French, V. Sobolev, *Physical Review B* **2005**, *71*(10), 104201.

[93] W. Bauhofer, J. Z. Kovacs, *Compos. Sci. Technol.* **2009**, *69*, 1486–1498.

[94] I. Balberg, N. Binenbaum, *Physical Review B* **1983**, *28*(7), 3799.

[95] M. Biercuk, M. C. Llaguno, M. Radosavljevic, J. Hyun, A. T. Johnson, J. E. Fischer, *Applied Physics Letters* **2002**, *80*(15), 2767–2769.

[96] Z. Yao, C. L. Kane, C. Dekker, *Physical Review Letters* **2000**, *84*(13), 2941.

[97] A. Znidarsic, A. Kaskela, P. Laiho, M. Gaberscek, Y. Ohno, A. G. Nasibulin, E. I. Kauppinen, A. Hassanien, *The Journal of Physical Chemistry C* **2013**, *117*(25), 13324–13330.

[98] N. Hu, Y. Karube, C. Yan, Z. Masuda, H. Fukunaga, *Acta Materialia* **2008**, *56*(13), 2929–2936.

[99] J. G. Simmons, G. J. Unterkofler, W. W. Allen, *Appl. Phys. Letters* **1963**, *2*.

[100] B. e. Kilbride, J. Coleman, J. Fraysse, P. Fournet, M. Cadek, A. Drury, S. Hutzler, S. Roth, W. Blau, *Journal of Applied Physics* **2002**, *92*(7), 4024–4030.

[101] M. Bryning, M. Islam, J. Kikkawa, A. Yodh, *Adv. Mater.* **2005**, *17*(9), 1186–1191.

[102] A. W. Musumeci, G. G. Silva, J.-W. Liu, W. N. Martens, E. R. Waclawik, *Polymer* **2007**, *48*(6), 1667–1678.

[103] E. Kymakis, G. A. J. Amaratunga, *J. Appl. Phys.* **2006**, *99*(8), 084302.

[104] J. Dai, Q. Wang, W. Li, Z. Wei, G. Xu, *Materials letters* **2007**, *61*(1), 27–29.

[105] V. Antonucci, G. Faiella, M. Giordano, L. Nicolais, G. Pepe, in *Macromolecular Symposia*, Wiley Online Library, volume 247 **2007** 172–181.

[106] Y.-T. Kim, C.-K. Baek, *Journal of Polymer Science Part B: Polymer Physics* **2003**, *41*(13), 1572–1577.

[107] P. Beecher, P. Servati, A. Rozhin, A. Colli, V. Scardaci, S. Pisana, T. Hasan, A. Flewitt, J. Robertson, G. Hsieh, et al., *Journal of Applied Physics* **2007**, *102*(4), 043710.

[108] W. R. Small, et al., *Small* **2007**, *3*(9), 1500–1503.

[109] J.-U. Park, M. Hardy, S. J. Kang, K. Barton, K. Adair, D. kishore Mukhopadhyay, C. Y. Lee, M. S. Strano, A. G. Alleyne, J. G. Georgiadis, et al., *Nature materials* **2007**, *6*(10), 782–789.

[110] J. Vaillancourt, H. Zhang, P. Vasinajindakaw, H. Xia, X. Lu, X. Han, D. C. Janzen, W.-S. Shih, C. S. Jones, M. Stroder, et al., *Applied Physics Letters* **2008**, *93*(24), 243301.

[111] N. Rouhi, D. Jain, P. J. Burke, *ACS Nano* **2011**, *5*(11), 8471–8487.

[112] E. Kymakis, P. Servati, P. Tzanetakis, E. Koudoumas, N. Kornilios, I. Rompogiannakis, Y. Franghiadakis, G. A. J. Amaratunga, *Nanotechnology* **2007**, *18*(43), 435702.

[113] P. N. Nirmalraj, P. E. Lyons, S. De, J. N. Coleman, J. J. Boland, *Nano Lett.* **2009**, *9*(11), 3890–3895.

[114] K. J. Zhang, A. Yadav, K. H. Kim, Y. Oh, M. F. Islam, C. Uher, K. P. Pipe, *Adv. Mater.* **2013**, *25*(21), 2926–2931.

[115] K. Mustonen, P. Laiho, A. Kaskela, T. Susi, A. Nasibulin, E. Kauppinen, *Applied Physics Letters* **2015**, *107*(14), 143113.

[116] M. Shimizu, S. Fujii, T. Tanaka, H. Kataura, *The Journal of Physical Chemistry C* **2013**, *117*(22), 11744–11749.

[117] N. Boulanger, J. Yu, D. R. Barbero, *Nanoscale* **2014**, *6*(20), 11633–11636.

[118] D. R. Barbero, N. Boulanger, M. Ramstedt, J. Yu, *Advanced Materials* **2014**, *26*(19), 3111–3117.

[119] N. Boulanger, D. R. Barbero, *Advanced Electronic Materials* **2015**, *1*(5).

[120] D. R. Boulanger, N. & Barbero, *in preparation* **2015**.

[121] M. Batzill, U. Diebold, *Progress in Surface Science* **2005**, *79*, 47–154.

[122] T. M. Barnes, J. D. Bergeson, R. C. Tenent, B. A. Larsen, G. Teeter, K. M. Jones, J. L. Blackburn, J. van de Lagemaat, *Applied Physics Letters* **2010**, *96*(24), 243309.

[123] Z. Wu, Z. Chen, X. Du, J. M. Logan, J. Sippel, M. Nikolou, K. Kamaras, J. R. Reynolds, D. B. Tanner, A. F. Hebard, A. G. Rinzler, *Science* **2004**, *305*(5688), 1273–1276.

[124] X. Li, Y. Jung, K. Sakimoto, T.-H. Goh, M. A. Reed, A. D. Taylor, *Energy & Environmental Science* **2013**, *6*(3), 879–887.

[125] S. Nanot, A. W. Cummings, C. L. Pint, A. Ikeuchi, T. Akiho, K. Sueoka, R. H. Hauge, F. Leonard, J. Kono, *Scientific Reports* **2013**, *3*, 1335.

[126] M. Mahjouri-Samani, Y. S. Zhou, X. N. He, W. Xiong, P. Hilger, Y. F. Lu, *Nanotechnology* **2013**, *24*(3), 035502.

[127] Z. Yang, T. Chen, R. He, H. Li, H. Lin, L. Li, G. Zou, Q. Jia, H. Peng, *Polymer Chemistry* **2013**, *4*(5), 1680–1684.

[128] F. Li, Z. Lin, B. Zhang, C. Wu, C. Hong, T. Guo, *Thin Solid Films* **2012**, *525*, 93–96.

[129] B. R. Lee, J. S. Kim, Y. S. Nam, H. J. Jeong, S. Y. Jeong, G.-W. Lee, J. T. Han, M. H. Song, *Journal of Materials Chemistry* **2012**, *22*(40), 21481–21486.

[130] J. Li, L. Hu, L. Wang, Y. Zhou, G. Grüner, T. J. Marks, *Nano letters* **2006**, *6*(11), 2472–2477.

[131] G. D. M. Dabera, K. I. Jayawardena, M. R. Prabhath, I. Yahya, Y. Y. Tan, N. A. Nismy, H. Shiozawa, M. Sauer, G. Ruiz-Soria, P. Ayala, et al., *ACS nano* **2012**, *7*(1), 556–565.

[132] D. S. Hecht, A. M. Heintz, R. Lee, L. Hu, B. Moore, C. Cucksey, S. Risser, *Nanotechnology* **2011**, *22*(7), 075201.

[133] A. A. Green, M. C. Hersam, *Nano letters* **2008**, *8*(5), 1417–1422.

[134] M. Kaempgen, G. Duesberg, S. Roth, *Applied Surface Science* **2005**, *252*(2), 425–429.

[135] M. A. Topinka, M. W. Rowell, D. Goldhaber-Gordon, M. D. McGehee, D. S. Hecht, G. Gruner, *Nano Lett.* **2009**, *9*(5), 1866–1871.

[136] G. Dabera, M. Prabhath, K. T. Lai, K. Jayawardena, F. L. M. Sam, L. J. Rozanski, A. Adikaari, S. R. P. Silva, *Advanced Functional Materials* **2015**, *25*(28), 4520–4530.

[137] S. H. Kim, W. Song, M. W. Jung, M.-A. Kang, K. Kim, S.-J. Chang, S. S. Lee, J. Lim, J. Hwang, S. Myung, et al., *Advanced Materials* **2014**, *26*(25), 4247–4252.

[138] M. A. Contreras, T. Barnes, J. van de Lagemaat, G. Rumbles, T. J. Coutts, C. Weeks, P. Glatkowski, I. Levitsky, J. Peltola, D. A. Britz, *The Journal of Physical Chemistry C* **2007**, *111*(38), 14045–14048.

[139] T. M. Barnes, X. Wu, J. Zhou, A. Duda, J. van de Lagemaat, T. J. Coutts, C. L. Weeks, D. A. Britz, P. Glatkowski, *Applied Physics Letters* **2007**, *90*(24), 243503.

[140] F. Wang, D. Kozawa, Y. Miyauchi, K. Hiraoka, S. Mouri, Y. Ohno, K. Matsuda, *Nat Commun* **2015**, *6*, 6305.

[141] J. Chen, K. Li, Y. Luo, X. Guo, D. Li, M. Deng, S. Huang, Q. Meng, *Carbon* **2009**, *47*(11), 2704 – 2708.

[142] A. Kongkanand, R. M. Dominguez, P. V. Kamat, *Nano Letters* **2007**, *7*(3), 676–680, pMID: 17309316.

[143] M. Hosoya, H. Oooka, H. Nakao, T. Gotanda, S. Mori, N. Shida, R. Hayase, Y. Nakano, M. Saitol, *Proceedings of the 93rd Annual Meeting of the Chemical Society of Japan* **2013**, 2137.

[144] S. Chaudhary, H. W. Lu, A. M. Müller, C. J. Bardeen, M. Ozkan, *Nano Lett.* **2007**, *7*, 1973–1979.

[145] E. Kymakis, M. M. Stylianakis, G. D. Spyropoulos, E. Stratakis, E. Koudoumas, C. Fotakis, *Solar Energy Materials and Solar Cells* **2012**, *96*, 298 – 301.

[146] E. Kymakis, G. A. J. Amaratunga, *Appl. Phys. Lett.* **2002**, *80*, 112–114.

[147] E. Kymakis, I. Alexandrou, G. A. J. Amaratunga, *J. Appl. Phys.* **2003**, *93*, 1764.

[148] A. T. Mallajosyula, S. S. K. Iyer, B. Mazhari, *J. Appl. Phys.* **2010**, *108*, 094902.

[149] J. Arranz-Andrés, W. J. Blau, *Carbon* **2008**, *46*, 2067 – 2075.

[150] S. Kazaoui, N. Minami, B. Nalini, Y. Kim, K. Hara, *J. Appl. Phys.* **2005**, *98*, 084314.

[151] E. Kymakis, E. Koudoumas, I. Franghiadakis, G. A. J. Amaratunga, *J. Phys. D-Appl. Phys.* **2006**, *39*, 1058–1062.

[152] J. X. Geng, T. Y. Zeng, *J. Am. Chem. Soc.* **2006**, *128*, 16827 – 16833.

[153] D. J. Bindl, M. Y. Wu, F. C. Prehn, M. S. Arnold, *Nano Lett.* **2011**, *11*, 455–460.

[154] S. Ren, M. Bernardi, R. R. Lunt, V. Bulovic, J. C. Grossman, S. Gradeak, *Nano Letters* **2011**, *11*, 5316–5321.

[155] M. J. Shea, M. S. Arnold, *Applied Physics Letters* **2013**, *102*(24), 243101.

[156] M. Gong, T. A. Shastry, Y. Xie, M. Bernardi, D. Jasion, K. A. Luck, T. J. Marks, J. C. Grossman, S. Ren, M. C. Hersam, *Nano Letters* **2014**, *14*(9), 5308–5314.

[157] S. N. Habisreutinger, T. Leijtens, G. E. Eperon, S. D. Stranks, R. J. Nicholas, H. J. Snaith, *Nano Letters* **2014**, *14*(10), 5561–5568.

[158] S. N. Habisreutinger, T. Leijtens, G. E. Eperon, S. D. Stranks, R. J. Nicholas, H. J. Snaith, *The Journal of Physical Chemistry Letters* **2014**, *5*(23), 4207–4212, pMID: 26278955.

[159] K. Aitola, K. Sveinbjornsson, J.-P. Correa-Baena, A. Kaskela, A. Abate, Y. Tian, E. M. J. Johansson, M. Gratzel, E. I. Kauppinen, A. Hagfeldt, G. Boschloo, *Energy Environ. Sci.* **2016**, –.

[160] Y. Kanai, J. C. Grossman, *Nano Lett.* **2008**, *8*, 908 – 912.

[161] T. Clarke, A. Ballantyne, F. Jamieson, C. Brabec, J. Nelson, J. Durrant, *Chem. Commun.* **2009**, *1*, 89–91.

[162] L. M. Liu, W. E. Stanchina, G. Y. Li, *Appl. Phys. Lett.* **2009**, *94*, 233309.

[163] B. Shan, K. Cho, *Physical review letters* **2005**, *94*(23), 236602.

[164] W. L. Abeygunasekara, P. Hiralal, L. Samaranayake, C.-T. Chien, A. Kumar, A. J. Flewitt, V. Karunaratne, G. A. Amaratunga, *Applied Physics Letters* **2015**, *106*(12), 123305.

[165] D. J. Bindl, N. S. Safron, M. S. Arnold, *ACS Nano* **2010**, *4*, 5657–5664.

[166] Y. Ye, D. J. Bindl, R. M. Jacobberger, M.-Y. Wu, S. S. Roy, M. S. Arnold, *Small* **2014**, *10*(16), 3299–3306.

[167] R. Ihly, K. S. Mistry, A. J. Ferguson, T. T. Clikeman, B. W. Larson, O. Reid, O. V. Boltalina, S. H. Strauss, G. Rumbles, J. L. Blackburn, *Nature Chemistry* **2016**.

[168] S. D. Stranks, H. J. Snaith, *Nat. Nanotechnol.* **2015**, *10*, 391–402.

[169] S. D. Wolf, J. Holovsky, S.-J. Moon, P. Lper, B. Niesen, M. Ledinsky, F.-J. Haug, J.-H. Yum, C. Ballif, *The Journal of Physical Chemistry Letters* **2014**, *5*(6), 1035–1039, pMID: 26270984.

[170] F. Deschler, M. Price, S. Pathak, L. E. Klintberg, D.-D. Jarausch, R. Higler, S. Httner, T. Leijtens, S. D. Stranks, H. J. Snaith, M. Atatre, R. T. Phillips, R. H. Friend, *The Journal of Physical Chemistry Letters* **2014**, *5*(8), 1421–1426, pMID: 26269988.

[171] A. Miyata, A. Mitioglu, P. Plochocka, O. Portugall, J. T.-W. Wang, S. D. Stranks, H. J. Snaith, R. J. Nicholas, *Nature Physics* **2015**, *11*(7), 582–587, pMID: 26270984.

[172] S. D. Stranks, G. E. Eperon, G. Grancini, C. Menelaou, M. J. P. Alcocer, T. Leijtens, L. M. Herz, A. Petrozza, H. J. Snaith, *Science* **2013**, *342*(6156), 341–344.

[173] W. Chen, Y. Wu, Y. Yue, J. Liu, W. Zhang, X. Yang, H. Chen, E. Bi, I. Ashraful, M. Grtzel, L. Han, *Science* **2015**, *350*(6263), 944–948.

[174] Z. Li, P. P. Boix, G. Xing, K. Fu, S. A. Kulkarni, S. K. Batabyal, W. Xu, A. Cao, T. C. Sum, N. Mathews, L. H. Wong, *Nanoscale* **2016**, –.

[175] A. Mei, X. Li, L. Liu, Z. Ku, T. Liu, Y. Rong, M. Xu, M. Hu, J. Chen, Y. Yang, M. Grätzel, H. Han, *Science* **2014**, *345*(6194), 295–298.

[176] X. Li, M. Tschumi, H. Han, S. S. Babkair, R. A. Alzubaydi, A. A. Ansari, S. S. Habib, M. K. Nazeeruddin, S. M. Zakeeruddin, M. Grtzel, *Energy Technology* **2015**, *3*(6), 551–555.

[177] Z. Li, S. A. Kulkarni, P. P. Boix, E. Shi, A. Cao, K. Fu, S. K. Batabyal, J. Zhang, Q. Xiong, L. H. Wong, N. Mathews, S. G. Mhaisalkar, *ACS Nano* **2014**, *8*(7), 6797–6804, pMID: 24924308.

[178] M. Cai, V. T. Tiong, T. Hreid, J. Bell, H. Wang, *J. Mater. Chem. A* **2015**, *3*, 2784–2793.

[179] X. Wang, Z. Li, W. Xu, S. A. Kulkarni, S. K. Batabyal, S. Zhang, A. Cao, L. H. Wong, *Nano Energy* **2015**, *11*, 728 – 735.

[180] I. Jeon, T. Chiba, C. Delacou, Y. Guo, A. Kaskela, O. Reynaud, E. I. Kauppinen, S. Maruyama, Y. Matsuo, *Nano Letters* **0**, *0*(0), null, pMID: 26327329.

[181] P. Schulz, A.-M. Dowgiallo, M. Yang, K. Zhu, J. L. Blackburn, J. J. Berry, *The Journal of Physical Chemistry Letters* **0**, *7*(0), 418–425, pMID: 26757105.

[182] H. J. Snaith, *The Journal of Physical Chemistry Letters* **2013**, *4*(21), 3623–3630.

[183] P. Loper, B. Niesen, S.-J. Moon, S. Martin De Nicolas, J. Holovsky, Z. Remes, M. Ledinsky, F.-J. Haug, J.-H. Yum, S. De Wolf, C. Ballif, *Photovoltaics, IEEE Journal of* **2014**, *4*(6), 1545–1551.

[184] J. P. Mailoa, C. D. Bailie, E. C. Johlin, E. T. Hoke, A. J. Akey, W. H. Nguyen, M. D. McGehee, T. Buonassisi, *Applied Physics Letters* **2015**, *106*(12), 121105.

[185] C. D. Bailie, M. G. Christoforo, J. P. Mailoa, A. R. Bowring, E. L. Unger, W. H. Nguyen, J. Burschka, N. Pellet, J. Z. Lee, M. Gratzel, R. Noufi, T. Buonassisi, A. Salleo, M. D. McGehee, *Energy Environ. Sci.* **2015**, *8*, 956–963.

[186] G. E. Eperon, V. M. Burlakov, A. Goriely, H. J. Snaith, *ACS Nano* **2014**, *8*(1), 591–598, pMID: 24467381.

[187] G. E. Eperon, D. Bryant, J. Troughton, S. D. Stranks, M. B. Johnston, T. Watson, D. A. Worsley, H. J. Snaith, *The Journal of Physical Chemistry Letters* **2015**, *6*(1), 129–138, pMID: 26263101.